Sizing of flaws using ultrasonic bulk wave testing: A review

Maria V. Felice, Zheng Fan *

School of Mechanical and Aerospace Engineering, Nanyang Technological University, 50 Nanyang Avenue, Singapore 639798, Singapore

A B S T R A C T

Ultrasonic testing is a non-destructive method that can be used to detect, locate and size flaws. The purpose of this paper is to review techniques that utilise ultrasonic bulk waves to size flaws. Flaws that are embedded within a component (i.e. remote from any surface) as well as flaws growing from inaccessible surfaces are considered. The different available techniques are grouped into the following categories: amplitude, temporal, imaging and inversion. The principles, applications and limitations of the different techniques are covered, as well as approaches to assessing the performance of the techniques. Finally, remaining gaps and challenges in sizing flaws, particularly in an industrial setting, are discussed.

© 2018 Elsevier B.V. All rights reserved.

Contents

---

* Corresponding author.
  E-mail address: zfan@ntu.edu.sg (Z. Fan).

1. Introduction

1.1. Motivation for flaw measurement

In the past few decades, there has been a shift from non-destructive testing to *quantitative* non-destructive evaluation (NDE) [1]. This is because flaws are no longer accepted or rejected based on 'workmanship' criteria, i.e. what the inspection system can detect, but based on 'Fitness-for-Service' criteria or Engineering Critical Assessment [2]. This has been driven by cost reduction in life management of structures, but quantitative NDE can also provide economic benefits during manufacture by controlling processes better [1].

Engineering Critical Assessment (ECA), also known as Defect Assessment, is "the analysis of a defect in a component to establish whether the defect will cause failure of the component" [3]. There are various standards related to this, including *Guide to methods for assessing the acceptability of flaws (BS7910)* [4]. In order to perform ECA, it is of utmost importance that the flaw size is known, together with associated errors and confidence levels [3]. If the flaw size is not known, then the only reliable option is to reject the flawed component. If the flaw type is not known then the worst case scenario is assumed, which is often that the detected flaw is a surface-breaking crack growing in an unfavourable direction with respect to the loading [5]. Note that Defect Assessment can also be used "to establish the size of a defect that would threaten the integrity of the component" [3].

With quantitative NDE, if a flaw is detected and found to have an unacceptable size, there are various options of how to proceed, as listed in [3]. These include replacing or repairing the component in which the flaw is present; keeping the component in service (if the severity of the consequence of failure is deemed low enough); changing the mode of operation of the component; and performing a refined measurement of the flaw.

1.2. Suitability of ultrasonic testing

If the reader is not familiar with ultrasonic testing, various textbooks can be consulted, e.g. Chapter 3 in [6]. Ultrasonic testing is a suitable method for detecting and sizing flaws that are embedded or that are growing from inaccessible surfaces. There are various reasons for its suitability, including the following:

- Ultrasonic waves can propagate through thick, solid parts so ultrasonic testing is suitable for flaws far beneath the inspection surface, unlike methods which can only detect flaws on, or very close to, the inspection surface e.g. Eddy current testing (p.111f in [6]) and potential-drop techniques (p.113f in [6]); or methods which can only detect flaws on the inspection surface e.g. visual methods (p.1f in [6]) and penetrant testing (p.104f in [6]). In fact, when defect assessment calculations require a value for how far into a component a defect has grown, ultrasonic testing is the main method used [3].
- Ultrasonic testing can be used to detect various types of flaws, such as cracks and inclusions.
- Similarly, ultrasonic testing can be used on a wide range of materials, compared to methods like magnetic particle testing which require the component to be ferromagnetic (p.91f in [6]).
- Ultrasonic waves are inherently safe, compared to methods like radiography which uses ionising radiation and thus requires multiple types of protection (p.40f in [6]).
- 'Off-the-shelf' ultrasonic testing equipment is widely available and is often portable so is suitable for on-site testing, e.g. inspection of pipe welds on site (Chapter 13 in [7]).
- Various ultrasonic testing standards are in place, ensuring it can be used for critical parts e.g. ASTM E164-13: Standard practice

for contact ultrasonic testing of weldments [8] and ASTM E2700-14: Standard practice for contact ultrasonic testing of welds using phased arrays [9]. In particular industries, e.g. aerospace, specific techniques have been developed, together with procedures.

1.3. Purpose and scope of paper

In recent years, a substantial amount of research has been published on sizing flaws using ultrasonic testing. Some researchers have compared various techniques e.g. [2,10–13], but it seems to have been several years since a comprehensive review was published e.g. [14] in 1980 and [15] in 1978. Since then, a lot has changed in ultrasonic testing, in particular the adoption of ultrasonic array probes, which are probes consisting of multiple elements that can be individually controlled [16]. Also, as with all Engineering fields, advances in computing power have dramatically increased the range of algorithms that are feasible to implement in NDE.

In this paper, bulk wave testing is considered, not guided wave testing (p.35f in [17]) nor surface wave testing (p.34f in [17]). In most cases, pulse-echo testing, where the ultrasound is transmitted and received from the same side of the component, will be considered, since often there is only access to one side of a component, especially when it is in service. Through-transmission and resonance testing are not included in this paper. 'Through-transmission' or 'shadow' testing involves placing a probe on each of two opposite surfaces of a part and detecting and measuring flaws by the shadow that they generate (p.160 in [17]). Resonance testing involves applying continuous ultrasonic waves to a part and analysing the frequencies at which resonance occurs to determine properties of the part (p.233 in [17]).

There are a variety of ultrasonic testing approaches including: contact testing (p.266 in [17]); immersion testing or 'water delay line' testing (p.276 in [17]); air-coupled ultrasonic testing [18]; laser ultrasonic testing [19,20]; and Electromagnetic Acoustic Transducers (EMATs) (p.65f in [6], [21]). The first three all utilise piezoelectric transducers. In this paper, attention will not be paid to what type of testing approach is being used since in most cases the approaches differ in how the ultrasound is transmitted into and received from the component, and not in what can be done with the ultrasound. However, there are some important limitations, e.g. air-coupled ultrasonic testing suffers from low efficiency due to the large impedance difference [1].

According to ASTM E1316-17a [22], a flaw is defined as "an imperfection or discontinuity that may be detectable by non-destructive testing and is not necessarily rejectable", whilst a defect is defined as "one or more flaws whose aggregate size, shape, orientation, location, or properties do not meet specified acceptance criteria and are rejectable". 'Flaw' and 'defect' are sometimes used interchangeably, including in some of the references in this paper. This paper is not limited to one type of flaw although cracks will be given the most attention since they are sometimes considered the worst in terms of their effects on component life [23]; in particular surface-breaking cracks will be highlighted since these are of particular industrial interest [5]. The focus of this paper is on techniques which can determine the size of the flaws, however, if a particular technique can also be used to determine other features, such as flaw shape, this will be mentioned. The shape of a flaw, such as the aspect ratio or 'sharpness' of a void, can be relevant for fatigue life predictions [5].

Acoustic microscopes (also known as ultrasonic microscopes) are not covered in this paper but it is important to mention them. These are systems which typically utilise frequencies greater than 100 MHz, and thus generate very high-resolution ultrasonic images (p.255f in [17]). They consist of an acoustic probe; a

pulse-mode measurement system for transmitting and receiving signals; a mechanical system to align and move the component being tested; and a computer for controlling and processing [1].

The intended audience of this paper consists of two groups. The first group is researchers who are seeking an overview of flaw sizing techniques using ultrasonic testing and a reference list for further reading. The second group is engineers in industry who are also seeking an overview of flaw sizing techniques and in particular want to gain an appreciation of recent techniques that have not yet been adopted by industry.

1.4. Structure of paper

To facilitate easy reading of the paper, terms that are used throughout the paper to describe inspection set-ups and flaws are explained in Section 2. In Section 3 the different sizing techniques are described and discussed. The techniques are grouped into four: temporal, amplitude, imaging and inversion. The performance of the different sizing techniques is summarized in Section 3.5. In Section 4, different approaches for assessing the performance of the techniques are discussed. In Section 5 remaining gaps and challenges in sizing flaws are discussed.

2. Nomenclature

Fig. 1 shows the various parameters that will be used in this paper. They are all two-dimensional diagrams since most of this paper deals with two-dimensional testing and imaging, because this is currently much more common than three-dimensional testing and imaging.

Fig. 1a shows the parameters that will be used in this paper when describing the component and probe. The horizontal dimension is x, the vertical dimension is z and the third dimension (horizontal; out-of-plane) is y. The inspection surface is the surface on which the probe/s is/are placed and the back wall is the far surface beneath the inspection surface, and often parallel to it. The distance between these two surfaces is the thickness of the component. The length of the probe/s is measured along the inspection surface, in the x-z plane.

Fig. 1b shows the parameters that will be used to describe embedded flaws that are horizontal or near-horizontal. The depth of such a flaw is the distance between the centre of the flaw and the inspection surface, perpendicular to the inspection surface. The length of such a flaw is its longest dimension in the x-z plane. The angle of inclination of such a flaw is the angle that the flaw

makes with the horizontal (x-axis), often equivalent to the angle it makes with the inspection surface.

Fig. 1c shows the parameters that will be used to describe surface-breaking flaws and embedded, vertical or near-vertical flaws. The 'through-wall' size or extent is used to describe the perpendicular height of the flaw relative to the surface (inspection surface or nearest surface) and flaw 'height' is used to describe the dimension of the flaw along its face [3]. For flaws growing perpendicular to the surface, through-wall extent is equal to flaw height. 'Flaw depth' is sometimes used to refer to flaw through-wall extent or flaw height but this is not standard nomenclature nowadays. The angle of tilt of such a flaw is the angle it makes with the normal to the surface. Thus, if the surface is horizontal, the angle of tilt will be measured from the vertical. The length of such a flaw is its dimension along the surface of the part, i.e. in the x-y plane. For surface-breaking flaws, the surface which the flaw grows from is often – but not always – the back wall. The point where the flaw meets this surface is referred to as the flaw 'corner' or 'root'.

It is also important to note that the term 'scattering' will be used in this paper to refer to any ultrasonic waves coming from a flaw, i.e. both diffracted and specularly-reflected waves.

3. Sizing techniques

Ultrasonic sizing techniques can be broadly divided into four categories, as represented schematically in Fig. 2. They are:

(i) Amplitude techniques which involve measuring the amplitude of a signal from the flaw and using the amplitude value, and often other knowledge, to infer the flaw size. These techniques are discussed in detail in Section 3.1.

(ii) Temporal techniques in which the arrival time of one or more signals from the flaw are used to infer its size. These techniques are discussed in detail in Section 3.2.

(iii) Imaging techniques in which signals from the flaw are used to obtain a two-dimensional or three-dimensional representation of the region of interest and flaw sizes are inferred from this representation in various ways. These techniques are discussed in Section 3.3.

(iv) Inversion techniques in which signals from the flaw are inputted into algorithms which determine the physical properties of the flaw from which the signals originated. These techniques are discussed in Section 3.4.

3.1. Amplitude techniques

In this paper, 'amplitude techniques' encompass techniques where the size of a flaw is inferred from the amplitude of a scattered signal from the flaw and the use of other knowledge (e.g. charts, reference samples) as described below. Decibel drop techniques (p.78 in [6]) can also be classified as amplitude techniques but require scanning of a single-element probe, or use of an array probe; therefore these techniques have been placed in the 'Imaging' section of this paper (Section 3.3).

In amplitude techniques, the amplitude of a signal from the flaw is recorded and is compared to amplitudes from known reflectors in reference test pieces; these test pieces must match the component being tested in terms of material, surface finish, attenuation (which depends on manufacturing and heat treatment processes [24]), size and coupling conditions (p.7 in [25], p.78 in [6]). The approach is based on the assumption that the flaw of interest is smaller than the ultrasonic beam width and hence that the larger the flaw, the greater the proportion of the beam that it will intersect, hence scattering more ultrasonic energy [26]. Standard reflectors include side-drilled holes (p.7 in [25]), flat-bottomed holes
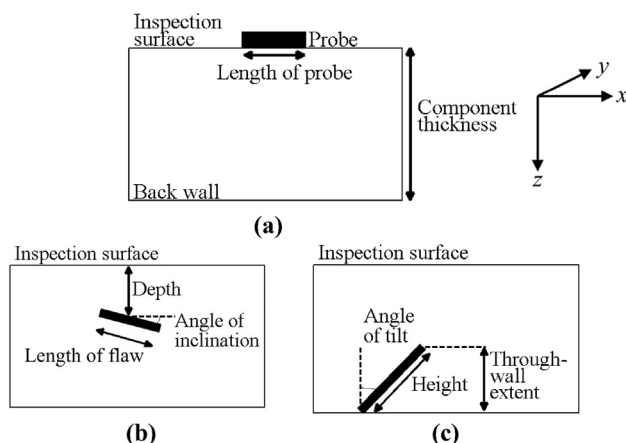

Fig. 1. Schematic showing parameters relevant (a) to the component and the probe; (b) to embedded horizontal or near-horizontal flaws; and (c) to surface-breaking flaws and to vertical or near-vertical embedded flaws. The axes shown in (a) are applicable to (b) and (c) too.
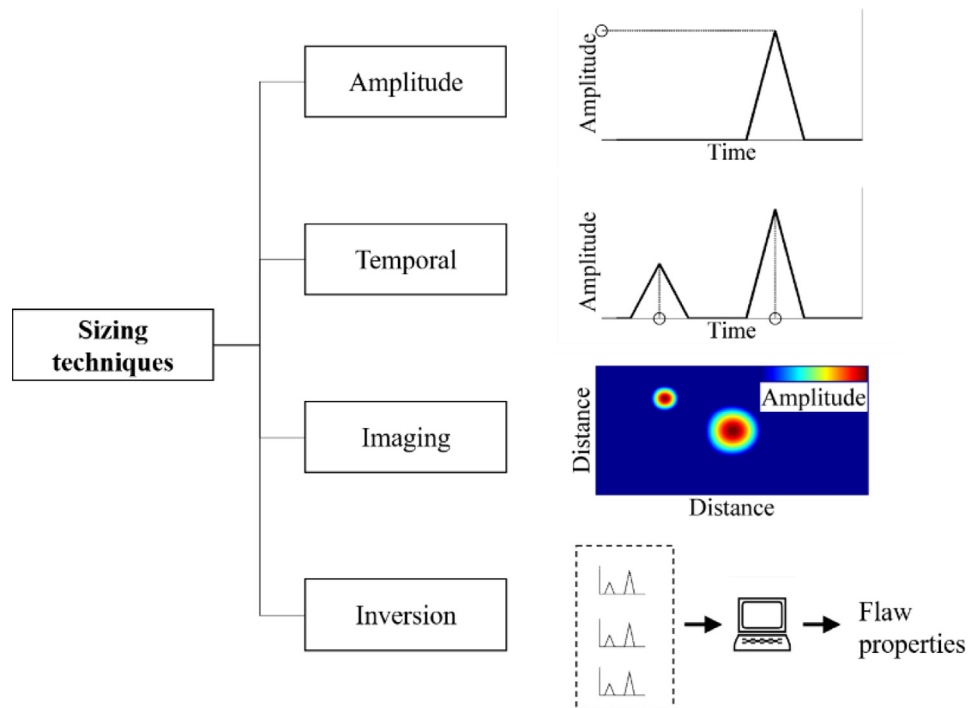
Fig. 2. Schematic showing the four main categories into which sizing techniques can be grouped.

[27]; or in the case of inspections for surface-breaking flaws, spark erosion slots and saw cuts can be used [15]. Test pieces with embedded solid reflectors can also be manufactured, for example by Hot Isostatic Pressing [28].

Distance-dependent thresholds or Distance-Amplitude-Correction curves can be used to account for the fact that the scattered amplitude from a reflector is dependent on its distance from the probe (p.182f in [17]). Distance-Amplitude-Correction (DAC) curves are plotted using standard reflectors at different depths in a reference part, making it a costly and time-consuming job (p.7 in [25]).

To avoid the need for physical test pieces, an alternative technique is to use a Krautkrämer AVG diagram [24]. This approach was originated by Krautkrämer [29] under the German title of *Abstand Verstärkung Größe* and the diagrams are also referred to as Distance-Gain-Size (DGS) scales [30]. Using the diagram corresponding to the specific probe and set-up, the scattered amplitude from a flaw is converted into the size of a circular flat reference reflector inspected at normal incidence (p.78 in [6]). This means that the true size of the flaw will be equal to or larger than this, and such information is of no use to 'Fitness-for-Service' criteria since it does not give a value for the maximum possible true size of the flaw [2].

Amplitude techniques are typically employed for flaws close to one wavelength in size where there is a monotonic relationship between flaw size and amplitude [31]. As flaws surpass a particular size, this relationship is no longer observed and this is true for various types of flaws [31], including the corner indication from surface-breaking flaws [32,33]. Furthermore, the monotonic relationship is not observed for flaws of all angles of inclination [31]. Also, for cracks of certain sizes, interference effects can come into play when reflections from different parts of the crack interfere, and this affects the relationship between amplitude and flaw size, leading to a cyclic response (with local maxima and minima) superimposed on a monotonic increase [26].

As well as the limits of validity just mentioned, a limitation with using amplitude techniques is that real flaws do not always scatter ultrasound in the same way as the reference flaws, which are often artificial flaws. For example, real flaws can be partially transparent to ultrasound (and thus scatter less ultrasound) for various reasons including: having small thicknesses (less than 0.5 μm thick will lead to severe transparency [34]); being full of material, such as oxides (p.106 in [17]); or having faces that are under pressure (p.106 in [17]). However, if the crack is under tensile load, it may give a larger response than when it is unloaded [35,36]. Fatigue cracks give a lower amplitude response than notches because of being semi-transparent and also because they can have rough surfaces; this can be dealt with by adding a predetermined amount of receiver gain when inspecting for fatigue cracks, so that the amplitude obtained can be compared to amplitude from notches [37]. Another way of overcoming the problem is to use cracks as the reference flaws, as has been done for stress corrosion cracking [38].

In the pipeline weld industry, when 'Fitness-for-Service' was adopted, flaw height measurements were required and the standard method used i.e. radiography could not measure this, so ultrasonic testing was adopted [2]. Initially amplitude techniques were used but these were found to be unreliable, so temporal techniques were used; and these will be discussed next.

3.2. Temporal techniques

The arrival time of a scattered pulse can be used to determine the location of the flaw, and this is often done in NDE, even when sizing is not required. The arrival time of scattering from two or more distinct points on an embedded flaw can be used to infer their respective locations, and hence the size of the flaw. If the flaw is surface-breaking then scattering from just one point can be sufficient since the second location equates to the known location of the surface.

A very common temporal technique is Time-of-Flight Diffraction (TOFD) which can be used to size embedded and surface-breaking flaws [34,39–42]. This technique relies on the diffracted signals from the extremity/extremities of the flaw, as represented
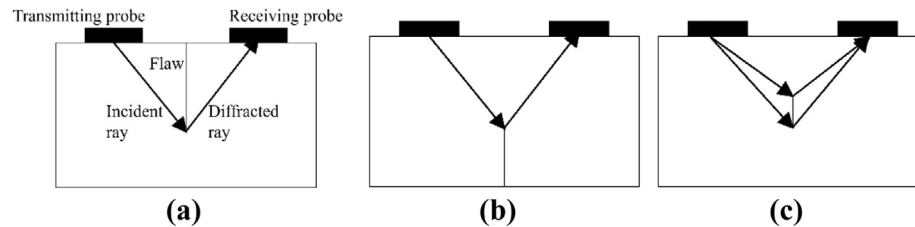
Fig. 3. Schematics showing the set-up and the ray paths to and from flaw tips in time-of-flight diffraction (TOFD) for (a) a surface-breaking flaw initiating from the inspection surface; (b) a surface-breaking flaw initiating from the back wall; and (c) an embedded flaw. The labelling in (a) is also applicable to (b) and (c).

schematically in Fig. 3. These signals are much lower in amplitude compared to specularly-reflected signals e.g. 20 dB less than the reflection from a 3 mm diameter side-drilled hole [43].

One of the earliest publications on TOFD is from 1975 [40]. In this publication, the TOFD technique is compared to an amplitude technique that had been presented recently in a conference paper by Böttcher, Schulz and Wustenberg, entitled *A new method of crack depth determination in ultrasonic materials testing*. The amplitude technique and TOFD both use the same set-up with a probe on either side of the flaw, placed on the surface from which the flaw originated (Fig. 3a). With Böttcher *et al.*'s amplitude technique, one probe transmitted ultrasound, the second probe picked up scattered ultrasound from the crack tip; and the scattered amplitude was used to determine the flaw through-wall extent. However the amplitude of the scattered ultrasound depended on coupling, angle of tilt of the crack and also on the presence of inclusions. Therefore a temporal technique with the same set-up was proposed where the arrival time of the scattering from the crack tip was used to determine its through-wall extent [40]. This technique was insensitive to coupling, angle of tilt and inclusions and it was found to give better and more consistent crack measurements compared to the amplitude technique. The diffraction response from a flaw is much less angular dependent than the specular response from a flaw [34].

With TOFD, only one diffraction signal is received from surface-breaking flaws; however there are additional observations. For a flaw that breaks the inspection surface, the indication of the lateral wave (which travels between the probes) will be affected; and for a flaw that breaks the back wall, the back wall indication will be affected [44].

In one quantitative study on steel blocks, TOFD was used to size machined slots of a range of through-wall extents using a 5 MHz probe [43]: it was found that the through-wall extent could be measured with mean error values of ±0.13 mm and ±0.06 mm for the vertical and tilted (10°; 15°) slots, respectively. In another study by the same authors [45] slots that were under cladding were measured using TOFD with a 4 MHz probe, and the through-wall extent was measured with mean error values of ±0.18 mm and ±0.14 mm for the vertical and tilted (10°; 15°) slots, respectively. The lengths of the flaws were also successfully measured with TOFD [43,45].

A good overview of the advantages and limitations of TOFD is given in [46] and the salient points are mentioned here. Since amplitude does not need to be measured and no comparative assessment needs to be made, consistent conditions are not as important for TOFD as for techniques which rely on amplitude measurement. The TOFD technique is often thought of as suitable only for cracks and similar flaws, but actually can be used for many flaw types. The lateral wave between the probes can cause problems since it will coincide with the diffracted signal from the nearest tip of near-surface embedded flaws. However, flaw signals from this region will be out of phase and superimposed on the lateral wave, so can still be detectable, although sizing will be less reliable than for flaws deeper in the component. Also, it is sometimes

possible to nullify the lateral wave since it is consistent. The TOFD technique is suitable even for flaws that are at large depths; in fact it can perform better for such flaws because the diffracted signals are more separated because of trigonometric displacement and it has been used for 250 mm thick parts. However, TOFD is probably less suited to coarse grain materials than other techniques because it is dependent on low-amplitude signals so is therefore affected a lot by attenuation.

It is common practice to scan probes when using the TOFD technique and generate displays or images of amplitude versus time and scan position [47]. An example set-up and image are shown in Fig. 4 for a steel component. The embedded, vertical flaw has a through-wall extent of 10 mm (z-direction) and a length of 20 mm (y-direction). Two probes of frequency 2 MHz and focused at 45° are used. The probes are positioned such that the flaw is centred between them in the x-direction; and they are scanned 100 mm in the y-direction such that they pass over the flaw in the centre of this scan. The ultrasonic data was simulated using the software package CIVA 2017 (EXTENDE S.A., Massy) and the image was plotted using this data.

Advances in TOFD are still being made, particularly in the areas of arrays and automation. The TOFD technique can be conducted using a phased array, either by using a long array and electronically scanning so that different groups of elements are transmitting and receiving [48] or by using a pair of array probes [10]. Researchers have looked into automating the interpretation and analysis of TOFD results [44,49–51]. For example, the various signals received during TOFD inspections have predictable phase differences, and automated algorithms can exploit the phase information to automatically identify and locate the different signals [44]. Another interesting development is the use of equivalent flaw TOFD (EFTOFD) where data is collected from multiple angles and used to determine an equivalent ellipsoid into which the flaw fits [52].

A second suitable temporal technique for surface-breaking flaws (typically cracks) is where the difference in arrival time between the corner (root) indication and the tip indication is used to determine the height of the crack [53], as shown in the schematic in Fig. 5. This technique has been referred to as the 'Relative Arrival Time Technique (RATT)' [11] but for simplicity will be referred to as the 'corner-tip' technique in this paper. This technique is employed with a probe placed above the flaw and to one side of it (not directly above it), so that the flaw is viewed at an angle. The tip indication is a result of tip diffraction, as with TOFD, although now it is back scatter as opposed to forward scatter [54]. Diffraction occurs at the corner because of the wedge formed between the component surface and the flaw; and if the flaw is normal (or near normal) to the surface then specular reflection will also occur at the corner [55]. The specular contribution is caused by two specular reflections – one on the component surface and one on the flaw surface. If the corner is 90° then the ultrasound is always sent back in the direction of incidence, irrespective of the direction [56].

As with TOFD, the corner-tip technique has been adopted using ultrasonic arrays too [57], but typically images are generated and
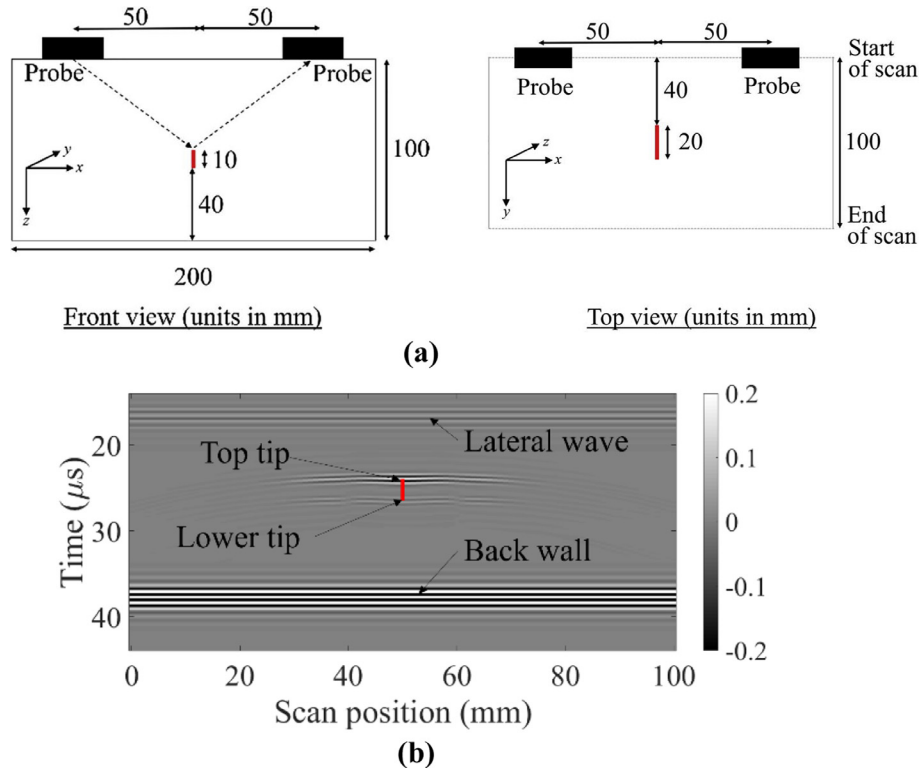
Fig. 4. (a) Schematic showing a set-up for a TOFD scan with two 2 MHz probes and (b) the resultant image with the flaw superimposed. The indications due to the lateral wave, back wall reflection, top tip diffraction and lower tip diffraction are marked in (b). The image in (b) was obtained using data simulated with CIVA (EXTENDE S.A., Massy). The flaw is shown as a red line in (a) and (b).
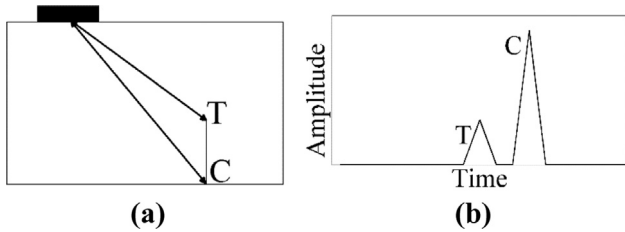

Fig. 5. Explanation of 'corner-tip' technique. (a) Schematic showing the ray paths between the probe and flaw tip (T) and between the probe and flaw corner (C); (b) Corresponding plot of amplitude versus time obtained from set-up in (a) showing two pulses or indications.

the distance between tip and corner indications is measured (Section 3.3.1) instead of measuring the time difference between the pulses in a signal.

As mentioned above, the specular contribution from the corner involves two reflections and both of these involve a phase change of 180° (total of 360°) since the wave is travelling in a material of higher impedance to that of the material beyond the surface, which is assumed to be air. Most other indications, e.g. from the back wall, only involve one phase change of 180°. Therefore, the reflections from the corners are 180° out of phase with other reflections and this difference can be used to identify and isolate them [56].

Temporal techniques are easily implemented and little data needs to be stored. However, timing accuracy and resolution are required and various attempts have been made to improve these, and hence improve flaw size accuracy and resolution. This has been done for both TOFD and the corner-tip technique and some approaches are mentioned here. By using deconvolution with autoregressive spectral extrapolation, the uncertainty in timing, and in depth estimation, was reduced by approximately 80% [58]. Another group took a semi-empirical approach of Weiner filtering

with autoregressive spectral extrapolation [57]. For TOFD, the linear frequency modulation ('chirp') pulse coding technique has been used to improve resolution [59].

There are several drawbacks with using temporal techniques to size flaws, since they depend on locating flaw tips. As mentioned in the section on Amplitude techniques, if the crack tip is full of oxide or has a compressive stress on it, then it will not scatter ultrasound well, or at all [60]. If just the tip is blocked with oxide, a diffraction signal will be obtained from below the tip where it is free of oxide [61] so there is a risk of undersizing flaws. Another issue that can occur is when flaws or components are complex, so that multiple indications are obtained. For example, deep stress corrosion cracks (SCCs) tend to be branched so will have multiple tips [31]. However, this does not always cause a problem and SCCs have been sized successfully using tip diffraction [38,48]. In fact, the tip diffraction technique was found to be superior at sizing stress corrosion cracks, compared to amplitude-based sizing, both when using notches as reference flaws and when using stress corrosion cracks as reference flaws [38]. A final issue is that flaw indications might overlap each other and/or indications from the part surfaces, for example with the corner-tip technique if the flaw has a small height, the corner and tip indications might overlap [11].

3.3. Imaging techniques

In two dimensions, ultrasonic data collected from an ultrasonic probe, can be expressed as values, u, which are a function of time, t, transmitter position, x_T, and receiver position, x_R, i.e. $u(t, x_R, x_T)$; whilst an ultrasonic image consists of pixels of intensity, I, at positions (x, z) in the inspection space i.e. $I(x, z)$ [62]. The intensity of the pixels usually corresponds to signal amplitude, but signal phase can also be used, for example phase imaging has been used to assist with characterisation of flaws in composites [63].

There are several different ultrasonic imaging techniques and these are outlined in Sections 3.3.2–3.3.4. There are also different techniques to obtain flaw measurements from ultrasonic images, and these are outlined in Section 3.3.1, so that the reader has an understanding of them before reading about the different imaging techniques. The imaging and measurement techniques are summarised in Fig. 6.

3.3.1. Measurement from an image

As shown in Fig. 6, there are two main ways of measuring flaws from images: measuring the size of an indication and measuring the distance between indications. Furthermore, images can be further processed to extract more information, for example by fusing different images or fusing information from different images [64,65], but this is not discussed in this paper.

The size of a flaw cannot be measured directly from its indication in an image because the indications are not sharp enough, due to the limit of resolution which will be discussed later in this section. Instead, the size of an indication is commonly measured using the 6 decibels (dB) drop technique (p.78 in [6]). Two powers P_1 and P_2 are said to differ by n bels if $P_1/P_2 = 10^n$; since amplitude is proportional to the square root of power, two amplitudes A_1 and A_2 differ by n bels if $A_1/A_2 = 10^{n/2}$ (p.57 in [6]). This can be expressed as:

$$n = 2\log_{10}\frac{A_1}{A_2}\, bels \tag{1}$$

and since a decibel is one tenth of a bel, (1) can be expressed as:

$$n = 20\log_{10}\frac{A_1}{A_2}\, decibels \tag{2}$$

Therefore, '6 dB drop' or '−6 dB' corresponds to an amplitude A_1 that is approximately half that of A_2. When using a single-element probe, the reasoning behind the 6 dB drop technique is that when the probe is over the centre of the flaw the entire beam will be intersected, whilst when the probe is centred over the edge of the flaw, half of the beam will be intersected, so the scattered signal amplitude will be half what it was in the centre (p.78 in [6]). This is represented schematically in Fig. 7. The 6 dB drop technique is valid if the flaw is larger than the beam and if the ultrasound is scattered from all parts of the flaw by the same amount [14]. The 6
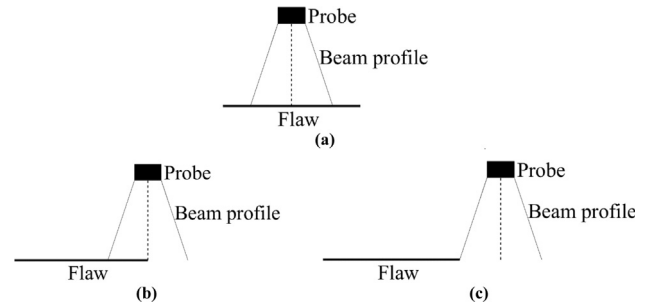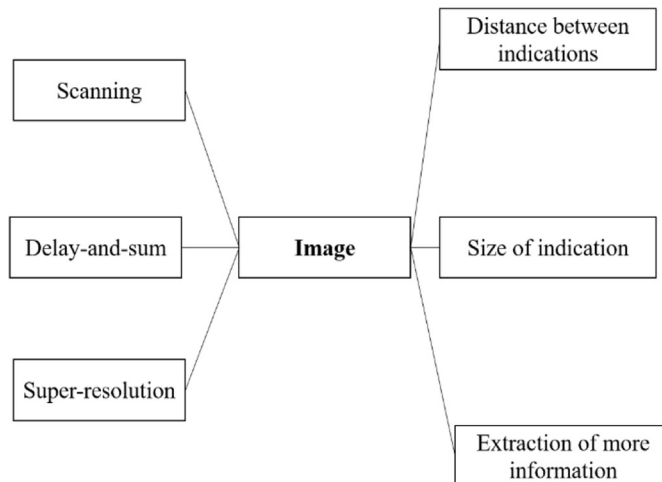

Fig. 7. Explanation of 6 dB drop and 20 dB drop sizing techniques. (a) Probe located above a flaw such that the entire beam is intersected by the flaw: in this position the maximum scattered amplitude (i.e. 0 dB) would be recorded. (b) Probe centred over the edge of a flaw such that half the width of the beam is intersected by the flaw: in this position half the maximum scattered amplitude (−6 dB) would be recorded. (c) Probe positioned such that that none of the beam is over the flaw (the edge of the beam is in line with the edge of the flaw): in this position hardly any scattered amplitude (−20 dB) would be recorded.

dB drop technique can be used on indications in A-scans (amplitude-time plots) or in images. When using images, it is the amplitude of pixels (often referred to as 'intensity') that is compared.

The dimensions of a flaw in different directions can be obtained by scanning along the different directions. However, it is important to remember that in the direction parallel to the ultrasonic beam, the dimension of the flaw indication is related to the ultrasonic pulse width and not the flaw size. For example, referring to Fig. 1a, if a probe with a vertical (z-direction) beam is scanned over a horizontal flaw in the x-direction, an indication in the x-z plane will be obtained: the x-dimension will correspond to the size of the flaw whilst the z-dimension will be related to the pulse width.

Other decibel drop techniques can be used, including the 20 dB drop technique, which corresponds to a 10× decrease in amplitude (compared to 2× decrease with 6 dB). The reasoning behind this technique is that when the amplitude has dropped by 20 dB, the flaw can be considered to be outside the ultrasonic beam (as shown in Fig. 7c); so the distance between the two points where the amplitude is 20 dB less than the maximum, corresponds to the length of the flaw plus the beam width (p.78 in [6]). Therefore,
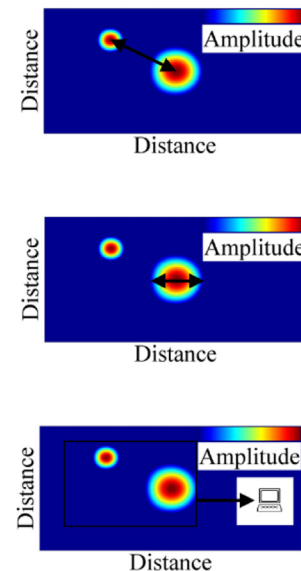

Fig. 6. Schematic showing different techniques of obtaining an ultrasonic image and different techniques of measuring flaws from these images.

using this technique it is possible to size flaws smaller than the beam width; however it is time-consuming since the beam profile at the flaw location must be known [14]. The third popular decibel drop technique is the 12 dB drop technique; for a detailed review and comparison of different decibel drop techniques, the reader is directed to [67]. An advantage of decibel drop techniques compared to amplitude techniques (i.e. measuring a single, maximum value) is that the former rely on relative amplitude values not absolute amplitude values, so do not require set-ups and conditions to be the same as for a reference test.

With single-element probes, if an attempt is made to use 6 dB drop sizing on flaws smaller than the beam width, what tends to happen is that the beam width is measured [2]. While this is obviously an inaccurate measurement, it can serve as a 'worst case' measurement because the flaw is actually smaller or equal to this size, and not greater than it. A similar observation is made with ultrasonic array probes, but with the size of the Point Spread Function (PSF) replacing the size of the beam width. The PSF is described later in this section.

A drawback of decibel drop techniques is that only the reflecting portion of the flaw is being measured. In some cases, the flaw will be oriented in such a way that only portions of it are scattering ultrasound back to the probe/s. However it is often the case that it is the extremities which are scattering ultrasound, e.g. as depicted in Fig. 5 for a surface-breaking flaw, so in such instances the flaw size can be inferred by measuring the distance between indications.

Measuring the distance between indications is similar in approach to temporal techniques, which also make use of the difference in arrival time of scattering from flaw extremities, but an image is often more intuitive to interpret than an A-scan or series of A-scans. The indications of the extremities of a small flaw will be very close to each other or even overlapping, and therefore the concept of limit of resolution is important when trying to locate these two extremities so that the flaw can be measured. Image resolution can be defined as the shortest separation distance between two points such that the amplitude between them drops to a particular threshold [68].

Before continuing with the discussion on resolution, it is important to mention the Point Spread Function. For any imaging system, even an infinitesimal scatterer will give an indication of a particular size; this is normally measured using the Point Spread Function (PSF) which is defined as the response of the imaging system to an ideal point scatterer [69]. The PSF originated from the field of optics, where it is defined as the finite-sized spread of flux obtained on an image plane when a single element is radiating flux; the flux is not focused to a point because of diffraction, and sometimes also aberrations (p.484f in [70]). The larger the PSF indication, the lower the resolution of the image and the further apart two points need to be so that their indications are 'resolvable'.

The resolution of an imaging system can be determined by simulating ultrasonic images of two ideal point scatterers and determining how close the scatterers can be such that they are still resolvable [71]; this separation will be the resolution. Most imaging algorithms are diffraction-limited which means the resolution obtainable in the lateral direction (perpendicular to the beam direction) cannot be better than that predicted using the Rayleigh criterion. In optics, the Rayleigh criterion states that the angular limit of resolution Φ_{min}, is:

$$\Phi_{min} \approx 1.22 \frac{\lambda}{D} \tag{3}$$

where λ is the wavelength and D is the lens diameter (p.222f in [72]). Lens diameter can be replaced by probe diameter for ultrasonic inspections. In two dimensions, the linear limit of resolution,

L_{min}, for an ultrasonic inspection set-up is given by the following expression [73]:

$$L_{min} \approx \frac{0.61\lambda}{\sin\theta} \tag{4}$$

or, by trigonometry : $L_{min} \approx 0.61\lambda \dfrac{\sqrt{\left(\frac{D}{2}\right)^2 + z^2}}{\frac{D}{2}}$

where D is the probe length, z is the vertical distance from the array to the region of interest, and θ is the angle between a vertical line from the centre of the probe to the region of interest and a line from the edge of the probe to the region of interest, as shown in Fig. 8.

There are some limitations when sizing flaws by measuring the distance between indications in an image. As mentioned, the smallest size that can be measured is limited by the resolution, which in turn is limited by the Rayleigh criterion unless super-resolution algorithms are used (Section 3.3.4). Also, it is essential that the two indications that are used correspond to the flaw extremities and it can sometimes be difficult to identify them. Typically, it is assumed that the strongest indications from the flaw will correspond to its tips, but this might not be the case, for example with stress corrosion cracks [33]. Also indications might be present at locations where there is no actual flaw; these might be due to multiple reflections from the flaw (or the component itself), or to more complex occurrences such as a bulk wave re-emitted from a creeping wave [74].

3.3.2. Scanning techniques

The simplest way of generating an image is to scan a single-element probe across a surface and collect a series of A-scans (plots of amplitude versus time) and use them to generate a B–scan or C–scan. A B-scan is a 2D image where the colour scale represents amplitude and two axes represent two dimensions - typically horizontal distance moved along the component and vertical distance (depth) into the part. A C–scan is also a 2D image but it represents a 3D volume; the two axes represent two horizontal dimensions whilst the colour scale represents a particular amplitude value obtained by considering all amplitude values through the depth e.g. maximum amplitude. To generate a B-scan, linear scanning is required, whilst to generate a C-scan, two-dimensional scanning, e.g. raster scanning, is required. More information and example images can be viewed in textbooks, e.g. p.84f in [6].

When scanning with a single-element probe, mechanical scanning is used i.e. the probe needs to be physically moved. When scanning with an array probe, electronic scanning can be used i.e. different elements of the array are used in turn, normally in sets (termed 'apertures') without moving the probe. A B–scan obtained by using different apertures of an array in turn is similar to a B-scan obtained when scanning a single-element probe whose diameter is equal to the array aperture [75]. Electronic scanning
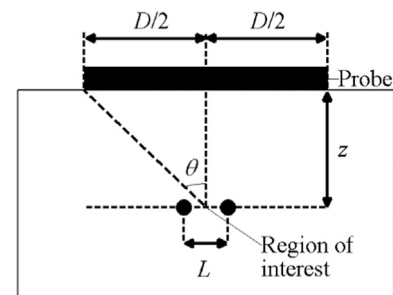

Fig. 8. Schematic showing variables used to compute the linear limit of resolution for an inspection set-up.

can be performed with or without mechanical scanning. Furthermore, electronic two-dimensional scanning is possible with an array; either fully electronically by using a 2D array or by electronically scanning along a linear array which is being mechanically scanned.

3.3.3. Delay-and-sum techniques

Delay-and-sum algorithms are those where each pixel in the final image has a value which is the "weighted sum of contributions from each signal in the raw data at specified points in time (the delays)" [76]. These algorithms therefore require multiple signals as input, either from one single-element probe that is being scanned, or more commonly nowadays, from ultrasonic array probes since these consist of multiple elements. Different delays are applied to the array elements both in transmission and reception. These enable ultrasonic beams to be focused at different locations and steered in different directions. Traditionally, focusing at different depths and angles was achieved using bespoke single-element probes e.g. with curved faces for depth focusing (p.193f in [17]) and plastic wedges for angle focusing (p.196f in [17]). The depth and angle would be fixed physical properties of the probe and/or wedge, unlike with delay-and-sum techniques were these can be changed. Delay-and-sum techniques are more advanced than scanning techniques, and the two can be combined [77].

When using ultrasonic arrays, there are two approaches to apply delays [75]. Actual 'physical' delays can be applied to the elements and this approach is referred to as 'beam forming', with elements transmitting in parallel with different delays. Alternatively, data can be collected from an array without applying any delays, and the delays can be applied 'synthetically' during post processing. This approach requires the collection of raw A-scans for different transmitter-receiver combinations. If all the transmitter-receiver combinations are collected, this is referred to as Full Matrix Capture (FMC) [75]. This is done in practice by transmitting on elements sequentially (one at a time), and collecting on all elements. It is useful to note that Full Raw Data (FRD) [78,79] is another approach in which all raw data is stored; the difference is that with FMC, only one element is transmitting at a time whilst with FRD multiple elements are transmitting at a time, so FMC is a special case of FRD [80].

The FMC matrix is an $N \times N$ matrix, where N is the number of elements, with each matrix entry containing a raw signal. As well as replicating traditional beam forming, FMC facilitates the application of imaging algorithms which would not be feasible with parallel transmission. Due to reciprocity of linear elastic systems, the signal when element i is transmitting and element j is receiving, u_{ij}, is equivalent to u_{ji}. Therefore, the full FMC matrix is not required and Half Matrix Capture (HMC), where $N(N + 1)/2$ signals are collected, does not lead to loss of information [76]. The HMC data can be used to populate the 'Full Matrix' for use in imaging algorithms. This means that despite there being no loss of information, there will be a reduction in signal-to-noise ratio because the same noise realisation is present in both u_{ij} and u_{ji} [76].

Different types of B-scans obtained using arrays are described in [75] and the salient points are mentioned here. A conventional B-scan or 'plane B-scan' was described in the previous section, and requires no delay laws. A 'focused' B-scan uses delays to focus at particular depths or points in the image space. If this is done using beamforming, different transmission cycles are needed for each focus depth or point, which is time-consuming, whilst if the FMC approach is used this can be done much more efficiently in post-processing. A sector B-scan is a type of image only easily obtained with an array, either using beamforming or the FMC approach. It is plotted in polar coordinates and each line corresponds to a particular angle of inspection and it differs from other B-scans because during beamforming all elements transmit together.

The Synthetic Aperture Focusing Technique (SAFT) originally involved scanning a single-element probe, collecting all the raw data and post-processing it; nowadays, the SAFT can be implemented with an array, using the data obtained when the same element is transmitting and receiving, i.e. the signals u_{ii} for $i = 1$ to N. [76]. The SAFT offers better lateral resolution than a B-scan [81] and can be considered similar to a focused B-scan, although the latter uses more transmitter-receiver combinations [75].

In one study, different techniques were used to image side-drilled holes of 1 mm diameter in aluminium with a 10 MHz array ($\lambda \approx 0.6$ mm) and it was found that the SAFT could size the holes more accurately than focusing at multiple depths ('Dynamic Depth Focusing'), which in turn performed better than focusing at a single depth [12].

The SAFT is also suitable for surface-breaking flaws and in one study with a single-element probe, the SAFT was found to be suitable for measuring the extent of vertical and tilted (10°; 15°) flaws under cladding [82]. In a previous study [45] by the same authors, that has already been discussed in this paper (Section 3.2), flaws less than 2 mm ($\lambda \approx 1.5$ mm) in through-wall extent were oversized using TOFD whilst these were sized more accurately using the SAFT [82]. In another study, it was found that the SAFT with a single-element probe (4 MHz; 45°) could be used to size notches on the back wall that extended 8% whilst B-scans generated using an array (also 4 MHz and focused at 45°) could be used to size notches that extended 6% [11].

The Total Focusing Method (TFM) [75] is a post-processing technique which uses the FMC data to generate an image as follows: delays are computed to and from all pixels such that ultrasound is synthetically focused at every pixel in the image space, hence the name 'total focusing'. The TFM has been successfully used to size embedded flaws larger than one wavelength by using the 6 dB drop technique and by measuring the distance between indications [66].

In array imaging, the Array Performance Index (API) is sometimes used as a measure of array performance, instead of the PSF. The API is equal to the area of the PSF (where the amplitude is within a particular threshold), divided by the wavelength squared (λ^2) [75]. The TFM has superior resolution to other delay-and-sum imaging algorithms and this has been demonstrated by comparing simulated API values (for a 6 dB threshold) for a point reflector beneath the centre of an array at a depth of 20λ: the API values obtained were as follows: 2.35 for plane B-scan; 1.71 for focused B-scan; 2.33 for sector B-scan and 0.46 for the TFM [75].

The Vector-TFM (VTFM) is an algorithm in which data from different apertures (sets of elements) of an array are used to determine the orientation of a flaw and this has been successfully done for flaws smaller than a wavelength [83].

Modifications to the TFM include the Half-Skip TFM (HSTFM) where ray paths include a skip off the back wall (in transmission or reception) [84–89] and the Full-Skip TFM (FSTFM) [84,87–89] where ray paths include a skip off the back wall in both transmission and reception. This means that the delays which are computed account for the extra travel time due to the skip/s off the back wall. Sometimes mode-converted signals are used; an example of this in the HSTFM could be the signal corresponding to a longitudinal wave transmitted from the array, a reflected shear wave from the back wall to the flaw and a direct shear wave from the flaw back to the array. This is done by using the appropriate velocities to compute the time delays corresponding to the different portions of the ray path. To differentiate it from the HSTFM and the FSTFM, the normal TFM is sometimes referred to as 'direct TFM' since the ray paths which are considered are those which go directly to and from the pixel.

When imaging surface-breaking cracks with the TFM using an array on the opposite surface to that from which the cracks grow there are two main locations to place the array. One is to place the array directly above the crack [85]: a weak tip indication will be observed which might overlap the back wall indication if the crack has a small height and a disruption in the back wall indication due to shadowing might also be observed. The more common approach is to place the array to one side of the crack so that a corner and tip indication are obtained. The through-wall extent of the crack can be measured by measuring the distance between these indications, but there are two main drawbacks to this technique [85]: the tip indication is very weak so might be invisible or obscured by noise; and when the crack has a small height, the tip and corner indications are likely to overlap.

The Half-Skip TFM has been found to be particularly good for imaging and sizing small surface-breaking cracks when the array is to one side of the flaw [85,90], as shown schematically in Fig. 9a. The main outputs from this work will be mentioned here. By using the HSTFM, specular reflections from all along the crack height are captured, so the crack is imaged along its entire height and the 6 dB drop technique can then be used to measure it. This has been done accurately in simulations (for cracks) and in experiments (for notches) when the through-wall extent is more than 1.5λ. However, as well as the lower limit, there is also an upper limit and cracks cannot be sized if their through-wall extent approaches the thickness of the component. One explanation for this is that no specular reflections from the top of the crack can be captured [33]. The solid arrows in Fig. 9a show specular reflection being captured from a point low down on the crack. The dashed lines in the same figure show how specular reflection cannot be captured from a point further up on the crack, for the same transmitting element. In addition to the issue just described, it is also possible that different portions of the crack receive different amounts of ultrasound (i.e. are insonified by different amounts). Therefore, in this case the 6 dB drop technique is invalid since it is based on the assumption that the ultrasonic beam is constant along the flaw.

As well as using 'skipping' to insonify flaw faces, skipping can also be used to insonify component surfaces (and flaws on these surfaces) that would not otherwise be in the required ultrasonic path, as shown in Fig. 9b for a weld. This is mentioned in standards for single-element probes [8] and ultrasonic array probes [9]. Researchers have also used array probes with skipping to collect FMC data from inaccessible locations [91,92]. The M-skip technique makes use of two single-element probes and multiple skips between them to inspect inaccessible portions of pipes and vessels [93].

Researchers have combined the information obtained from the TFM, the HSTFM and the FSTFM to determine the shape of small flaws [64], to image the top and bottom of a hole from one inspection surface [89] and to measure flaws of complicated shapes [94]. Combining these techniques has been referred to as multi-view TFM (MTFM) where a different technique is used to generate each image [64]; and Combined TFM (CTFM) where the techniques contribute to the same image [94]. 'Multi-mode TFM' was the original term used to refer to TFM using different wave modes (shear, longitudinal) and different ray paths [88].

In plane wave imaging (PWI), multiple elements transmit simultaneously to generate a plane wave at a particular angle [95]. This technique has been combined with TFM, by generating Q plane waves at different angles, receiving on all N elements, and using this $Q \times N$ matrix of data to focus at each pixel [96]. Fewer transmissions are required compared to performing FMC, but image quality is comparable to that from performing TFM with the full $N \times N$ matrix of data. As with TFM, PWI can be performed with skips, and surface-breaking cracks have been imaged well with this approach; importantly artefacts can be reduced since the angles of inspection can be controlled [96].

The wavenumber algorithm [97] and the back propagation algorithm [98] are similar to TFM in that they use FMC data to focus at all pixels. The wavenumber algorithm is more mathematically rigorous than the TFM, and provides a solution to the inverse problem for the assumed forward model of wave propagation [97]. The back propagation algorithm is based on the back propagation of the angular spectrum of transmit-receive signals [98]. To facilitate comparison, the TFM, wavenumber and back propagation algorithms were all expressed as frequency-domain delay-and-sum algorithms [62] (succinct comparison in [76]). The imaging performance of the algorithms was compared and it was found that back propagation and wavenumber algorithms gave very similar results, which sometimes superseded those from the TFM [62]. For example, when including low amplitudes (≈ -30 dB and less), the Array Performance Index was worse for the TFM than for other algorithms. Furthermore, grating lobes (unwanted indications on the sides of the image) were more visible in some TFM images, whilst they are filtered out with the other algorithms; however this filtering also means that flaws that are not directly beneath the centre of the array have lower amplitude indications than in the TFM. For practical purposes, the TFM is preferred because, at the expense of only slightly lower performance, it has the advantages of being suitable for all flaw shapes (unlike the wavenumber method), being very easy to implement, being able to cope with wave conversions and being computationally quick enough that it can cope with 2D arrays [62,68].

Inverse Wavefield Extrapolation (IWEX) [99,100] is similar to the back propagation algorithm but with the assumption that the inspection space is in the far field of the array elements [62]. Half-Skip and Full-Skip variations of the IWEX technique have been implemented, and they have been used together with direct IWEX to image stress corrosion cracks along their depth [65].

Classical delay-and-sum beam-forming algorithms are linear and non-linear denoising algorithms can be used to reduced uncorrelated material noise and improve image quality [68]. Such algorithms include phase coherence imaging [101] and spatial compounding [102]. These algorithms have been compared to the TFM and in terms of resolution, it was found that phase coherence imaging performed better than the TFM and spatial compounding performed worse than the TFM [68]. However, all techniques gave resolutions close to the Rayleigh limit of resolution, unlike super-resolution techniques which significantly overcome this limit and which will be discussed next.

Fig. 9. Skipping from the back wall (a) being used to capture specular reflections from a surface-breaking flaw; and (b) being used to insonify a weld surface. The solid arrows in (a) shows ray paths for a point low down on the flaw; whilst the dashed lines in (a) show ray paths for a point further up on the flaw, for which no ultrasound returns to the probe.

3.3.4. Super-resolution techniques

Most imaging algorithms are diffraction-limited which means that features on an object which are less than half a wavelength apart cannot be resolved, when scattering experiments are per-
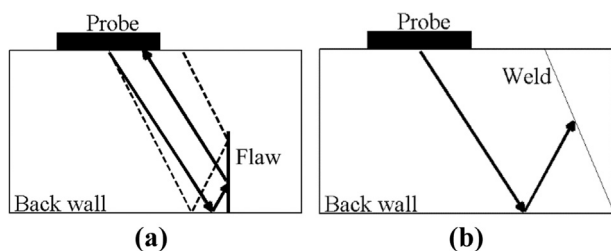
formed from the far field [103]. Super-resolution imaging algorithms can be used to overcome the diffraction limit and hence characterise sub-wavelength flaws [76]. As shown in Eq. (4) in Section 3.3.1, resolution improves as wavelength decreases, or frequency increases. However using a higher frequency is not always an option, for example, in attenuative materials high frequency waves do not propagate far [104] and when using multiple elements, the spacing between them should be less than $\lambda/2$ [105] so the higher the frequency the more challenging this becomes.

One super-resolution technique frequently used in ultrasonics is time-reversal MUSIC (TRM); where 'MUSIC' stands for MUltiple SIgnal Classification [106,107]. This technique has been compared to TFM [71] and it was found that when the time-domain signal-to-noise ratio (SNR) was greater than 20 dB, TRM gave higher lateral resolution and more compact point spread functions than TFM. For example, for one set-up, when the Rayleigh criterion was 1.5λ, the TRM algorithm was able to resolve two points that were 1.2λ apart with a drop in amplitude between the indications of approximately 25 dB. Such a drop in amplitude was seen with TFM when two points were separated by 2.6λ. However, as the SNR decreased the performance of TRM decreased, and its performance was very poor as the SNR fell below 5 dB. It is therefore recommended to monitor the SNR and use TFM if SNR is poor, since TFM is very robust even when SNR is 0 dB. A disadvantage of the TRM technique is that it requires *a priori* knowledge that the scatterers are point-like [108]. Note that, TRM has now been extended to arbitrary shaped scatterers [106].

The Born approximation neglects distortion (due to multiple scattering) of the probing wave as it travels through the object being imaged because the assumption is that the object is weakly scattering [103,108]. This approximation is often adopted in imaging algorithms but the neglected distortion can encode unlimited resolution so using the Born Approximation might be the reason for the diffraction limit [103]. The Linear Sampling Method (LSM; previously known as the 'simple method') [109,110] and the Factorisation Method (an improvement to the LSM) [111] are two techniques which do not utilise the 'weakly scattering' approximation, do not require any *a priori* knowledge about the scatterer and are non-iterative [104,112]. Using the Factorisation Method (FM) and experimental data, a resolution better than $\lambda/3$ has been obtained at a distance of 8λ from the receivers with a limited view [108]. Note that this study was performed with guided waves not bulk waves. Using bulk waves and a ring array (to achieve full view) a resolution better than $\lambda/4$ has been obtained at a distance of 70λ from the receivers, despite very high noise [103]. The LSM and FM have been used to image the contour of a kite-shaped hole that was approximately $3\lambda \times 3\lambda$ using simulated data; the FM provided a clearer image than the LSM with fewer artefacts [104]. The LSM was compared to beam-forming using experimental data from two human hairs; the resolution of the LSM images was superior to that of beam-forming and LSM was able to resolve the hairs when the distance between them was half the Rayleigh limit [104].

3.4. Inversion techniques

Scanning and delay-and-sum imaging techniques follow the sequence of: collect ultrasonic data, plot data in the form of an image and identify and analyse flaw indications in the image. When using inversion techniques, the logic is different: ultrasonic data is collected and by following one of many available algorithms, the physical properties of the flaw which gave rise to this data are inferred [76]. Inversion can be considered the 'opposite' of forward modelling where physical properties are inputted into a model and response data is outputted. Note that super-resolution imaging algorithms are also inversion techniques but

they were included in the previous section since they can also be classified as imaging algorithms.

3.4.1. Time-Reversal techniques

Time Reversal is a technique consisting of three steps: (i) signals are emitted from a source, (ii) scattered signals are received by receivers and reversed in time and (iii) the reversed signals are emitted from the source, to achieve focusing at the location of the scatterer [113–115]. The technique has the advantage of being able to focus through inhomogeneous media and it makes use of the linear response of transducers to pressure.

The term 'DORT' stands for *Décomposition de l'Opérateur de Retournement Temporel* in French, which is *Decomposition of the time-reversal operator* in English. Time Reversal traditionally focused on the strongest reflector in a group of reflectors whilst DORT is capable of focusing on multiple reflectors and theoretically can be considered as a generalisation of iterative Time Reversal techniques [116,117]. The DORT technique has been compared to the Total-Focusing Method (TFM) for imaging flaws in welds and the DORT technique exhibited a higher signal-to-noise ratio than the TFM; however the TFM was better at flaw characterisation [118]. The DORT was compared to Dynamic Depth Focusing (DDF) and the TFM for imaging flaws in parts whose inspection surface has a complex profile [119]. The component was tested in immersion so that there was a water path between the array and the inspection surface; and an advantage of DORT was that prior knowledge or computation of the profile was not required. However, a disadvantage was that it struggled to image small flaws close to interfaces, compared to the other two techniques [119]. This can be overcome using the 1-bit DORT technique which only retains the sign (+/-) of the received signal [120].

The time-reversal focusing technique (TRFT) is an iterative technique that locates crack tips by searching for a focal point common to the incident field and the corresponding time-reversed field from crack tip diffraction [13]. The TRFT was compared to the SAFT for evaluating surface-breaking cracks; and it was found that both the SAFT and the TRFT can estimate the depth of slits and open fatigue cracks with similar accuracy but when a crack is not completely open nor closed, the TRFT outperforms the SAFT [13].

Time-Reversal techniques can sometimes achieve 'super resolution'. This is because a pseudo-lens is created due to the interaction of the sound with the entire inhomogeneous mass and the diameter of this lens is greater than that of the physical array [117]. Therefore, the diffraction limit, as predicted by Eq. (4) with the physical array size, is exceeded.

3.4.2. Scattering matrix techniques

In the far field and for a given incident and scattered wave mode, the scattering amplitude and phase from a scatterer is a function of three variables: incident angle, scattered angle and frequency; and a scattering matrix (S–matrix) is a way of storing, or representing this information [121]. The S–matrix concept was first introduced to elastodynamics in 1978 [122]. An example S-matrix obtained by simulation is shown in Fig. 10 [123].

Scattering matrices have been used to store the ultrasonic scattering information from a flaw obtained by simulation [123–127]; this information can then be retrieved later for a particular inspection angle and frequency. This is particularly useful and intuitive when simulating ultrasonic array data since the different array elements view the flaw from different angles.

In two dimensions and in the frequency domain, the signal received at array element R when element T is transmitting, $U_{TR}(\omega)$, is given by the following equation [76]:

$$U_{TR}(\omega) = \frac{1}{\sqrt{d_T d_R}} U_0(\omega) D(\theta_T) D(\theta_R) S(\theta_T, \theta_R, \omega) e^{-ik(d_T + d_R)} \tag{5}$$
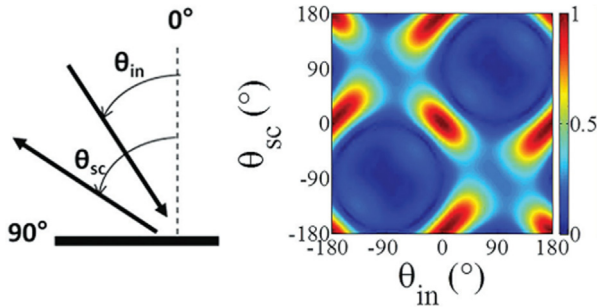
Fig. 10. A simulated S-matrix for a slot with a length of one wavelength. The colour scale represents scattered amplitude and is plotted against incident angle, θ_{in}, and scattered angle, θ_{sc}. This image is from [123].

where d is distance between the element and the flaw; $U_0(\omega)$ is the input spectrum; D is array element directivity; θ is the angle that a line between the array element and the flaw makes with the vertical; S is the scattering matrix; k being the wave number; e being the base of the natural logarithm and $i = \sqrt{-1}$. None of the parameters in this expression, except for S, are computationally intensive to determine. Therefore an efficient approach is to compute S once for a reasonable range of angles and frequencies, and then look up the necessary values when simulating data for different array and flaw locations (for which the other parameters will need to be computed each time).

Scattering matrices have also been used to characterise flaws and, like super-resolution imaging techniques, the aim of this approach is to characterise sub-wavelength flaws [76]. However instead of generating images which contain flaw indications, it is the S–matrices of flaws which are generated and analysed. Before describing different S–matrix characterisation techniques, it is useful to explain why S–matrices hold more information than delay-and-sum images, and this explanation is taken from [76]. Flaws which are large can be sized directly from an image, because different time delays are introduced when viewing the flaw from different angles by the phase gradients (with respect to frequency) in the flaw's S–matrix. However this phase gradient is very small for small flaws so the flaw appears in the image as a single point, similar to the PSF; the spatial information has been lost in delay-and-sum. The S–matrix characterisation approach seeks to retrieve the flaw size and shape from the S–matrix.

In one of the earliest publications on characterising flaws using S–matrices, the S–matrix was obtained using the sub-array approach i.e. by interrogating the flaw from different angles by using different sets of array elements [121]. The amplitude and location of the maximum value in the measured S–matrix were used to determine the flaw size and orientation respectively. In the experimental study, embedded flaws as small as $\approx 0.8\lambda$ were considered, and when the array was directly above the flaw the measured lengths had errors within 10% and measured angles were within a few degrees. In a later study by the same authors, the inverse back propagation algorithm was used to extract scattering from flaw [66]. In this work, the Half-Width at Half-Maximum (HWHM) was used to determine flaw size. The HWHM is half the angular range in the S–matrix for which the amplitude is within half the maximum value. With no noise, flaws as small as 0.2λ could be sized with this approach; when the relative noise was 10% flaws as small as 1.6λ could be sized.

Another technique by the same research group involves comparing the measured S–matrix from a crack-like flaw to a simulated library of S–matrices, using the Structural Similarity (SSIM) index [128]. This index is a quantitative way of comparing two images by comparing their luminance, contrast and structure [129]. The dynamic classifier approach [23] builds on this

technique (by incorporating other flaw types), as does the work in [130]. The recently proposed parametric-manifold mapping technique also uses scattering matrices, and importantly this technique has been used to measure surface-breaking flaws [5]. The surface-breaking flaws were notches with through-wall extents of 2 mm and 3 mm ($\lambda = 2.5$ mm) and angles of tilt that ranged from 0° to 45°. Note that the array was placed away from the flaw so that scattering from the back wall would not interfere with scattering from the flaw. An advantage of the technique is that it provides a measurement of the flaw characterisation uncertainty [5].

Another research group derived a relationship between the size of a crack and the maximum eigenvalue of the crack's S–matrix [131]. This technique does not require computation of a library of S–matrices and it was used to measure a crack whose length to wavelength ratio ranged from 0.6 to 1.9λ with an error of 12%. A sensitivity analysis showed that the technique is most effective for flaws in the order of one wavelength. The same research group used the relationship between the width of the central lobe of the S–matrix and the crack size to derive an analytical expression for crack length [132]. They found that this technique was not robust for experimental use. However, they used the model to develop an optimisation technique to determine the crack size for which the difference between simulated S–matrices (many sizes) and the measured S–matrix (single, true size) was smallest. This optimisation technique, over multiple frequencies, was tested experimentally on a crack of length 6 mm and the estimated length was 6.4 mm ($\lambda = 1.2$ mm).

Experimentally obtaining S–matrices from surface-breaking (or near-surface) flaws is a complex challenge because scattering from the back wall is received at the same time as scattering from the flaw. Nevertheless, the S–matrices from surface-breaking flaws were successfully extracted for surface-breaking flaws of length 2.3λ and through-wall extents of 1.1λ, 0.5λ and 0.2λ, using back wall elimination [133]. The study also included S–matrices obtained without back wall elimination and these results were significantly poorer.

3.4.3. Other inversion techniques

Some other inversion algorithms that have been recently used to characterise flaws in NDT include topological imaging [134] and Full Waveform Inversion [135,136]. These are both iterative techniques, where ultrasonic data is collected from a real component and compared to modelled data from a flaw-free component. If there is a flaw present in the real part, the two data sets will differ; and the model will be updated to reduce this difference. Eventually, the difference between the two data sets will be low, and if the technique is working properly, the model will now be a close representation of the real, flawed component. One group used a form of topological imaging with a single iteration to detect and locate surface-breaking flaw [137]. It is important to note that in some cases, the image obtained will not be of ultrasonic indications, but will represent the model e.g. velocity map in Full Waveform Inversion [135,136].

3.5. Summary

After comparing amplitude techniques, temporal techniques, imaging techniques and inversion techniques, some general comments can be made. Amplitude techniques can be used to measure flaws whose size is in the region of a wavelength but they are time-consuming to implement and, when comparing to a reference, the techniques are prone to failure if there are discrepancies between the reference measurement set-up and the test set-up. Furthermore if the flaw scattering is complicated e.g. from a multi-faceted flaw, the techniques are no longer valid. Temporal techniques do not require reference measurements so are more robust

to inconsistencies. They often rely on diffracted signals which are scattered in multiple directions making the techniques less sensitive to flaw orientation; however the diffracted signals tend to be weak and this lowers the sensitivity of the techniques. Temporal techniques are widely used in industry and mentioned in great detail in standards e.g. Time-of-Flight Diffraction (TOFD) [47] and Relative Arrival Time Technique [138].

Scanning imaging techniques are easy to implement, since they require a single-element probe or simple use of an array probe, however resolution can be limited. Delay-and-sum imaging algorithms offer better resolution and more flexibility but are still diffraction-limited. Super-resolution algorithms all overcome the diffraction limit but can be complicated to implement and some are only valid for certain types of flaws. Inversion techniques can also overcome the diffraction limit but again can be complicated to implement and can also be highly computationally intensive.

4. Assessment of sizing techniques

There are three aspects of an inspection technique that can be assessed: its sensitivity [139] (or the 'Probability of Detection (POD)' [1]), its ability to locate flaws [139] and its ability to size flaws [139]. Only techniques of assessing the sizing performance will be discussed here since they are most relevant to the theme of this paper. When assessing any aspect of an inspection technique, it is important that the flaw samples used are representative of the flaws that will actually be measured, since flaws differ from artificial reflectors such as notches, as mentioned in Section 3.1.

It is essential that the performance of flaw sizing techniques is assessed quantitatively. Incorrect sizing can have serious consequences; overestimating flaw sizes can result in unnecessary repairs which cause financial losses and may even introduce further flaws, whilst underestimating the size of a flaw can have serious effects on structural integrity [4].

If a flaw measurement, a_m, is obtained and the true size, a_t, of the flaw is known, then one way of determining the accuracy is as follows [35]:

$$Accuracy = 1 - \left| \frac{a_m - a_t}{a_t} \right| \qquad (6)$$

so that if $a_m = a_t$ then an accuracy value of unity is obtained.

Tests to determine the accuracy of flaw sizing can be carried out at the same time as POD studies: the component is cut open at the location where the flaw is detected, the flaw is sized visually and its true size compared to that obtained with the ultrasonic technique (p.163f in [7]). However, due to the large variation in parts and readings, error values determined in such a way cannot be deemed valid for all future inspections. Therefore, a statistical approach is taken by many standards (p.249 in [7]).

In a document by Britain's *Health and Safety Executive (HSE)* [3] look-up tables are mentioned for estimating the systematic and random errors; and a table is provide for the errors when measuring flaw through-wall extent using the maximum amplitude technique and when measuring flaw length using the 6 dB drop technique. For example, with the maximum amplitude technique, the standard deviation error for a flaw 20 mm away from the probe is given as ±3 mm. However, the document also refers to a more accurate approach where errors for a particular inspection are considered one by one, and an example of the application of this approach is given in [140]. Interestingly, the *HSE* document [3] was issued partly in response to studies which showed that for the same size flaw, a large range of sizes were recorded using ultrasonic sizing techniques.

Different inspection systems are available for industrial use, and for weld inspection it has been found that the variation from ultrasonic system to ultrasonic system is less than that from weld to weld or flaw to flaw; thus statistically, the different sizing techniques used by different service providers with different systems are approximately equal (p.249f in [7]).

Gauge R&R (repeatability and reproducibility) studies are a way of quantifying the performance of a measurement system by analysing the variation of measurements of a gauge (i.e. the repeatability) and the variation of measurements by operators (i.e. the reproducibility) (p.1 in [141]). Gauge R&R studies have been applied to quantitative ultrasonic testing; these two examples are for thickness measurement: [142,143].

Structural Similarity (SSIM) indices [129] can be used to compare Scattering Matrices [128,130] as mentioned in Section 3.4.2. The use of SSIM indices to compare ultrasonic images of flaws to the actual flaw is not recommended since there is a certain amount of 'blur' caused by diffraction and hence the PSF, so the flaw indication is larger than the flaw. Also, for volumetric flaws like pores, the centre of the pore will not show up in the ultrasonic image since it is only flaw edges that are represented. However, SSIM might be useful for comparing velocity maps obtained using FWI (Section 3.4.3) because in this technique, the whole area or volume of the flaw is represented in the resulting images.

5. Remaining gaps and challenges in sizing flaws

As seen in this paper, there are a lot of techniques available to size flaws using ultrasonic testing and research is constantly underway to be able to size smaller flaws. However, several challenges remain, in particular when it comes to considering non-ideal inspections. It is only natural that most researchers focus on simple, 'ideal' cases when developing a new sizing technique, but in real inspection scenarios, the flaws, material, part geometry and so on are non-ideal.

Most sizing techniques consider the case of single, isolated flaws, so that any scattered signals that are not from a component geometry have all originated from a single flaw. However, in reality, clustered flaws are not uncommon, for example inclusions [144] and cracks [60], including complex-shaped stress corrosion cracks [145], can occur as non-isolated flaws. Many small flaws near each other could be falsely interpreted as fewer flaws that are larger in size [146]. More work is needed to understand the effect of neighbouring flaws on the performance of sizing techniques.

It is often ideal flaws (strongly reflecting, smooth, straight etc.) that are considered when developing a new sizing technique. It would be of great benefit if developers of new sizing techniques could analyse the performance of their novel sizing technique for 'non-ideal' flaws. If the sizing technique works just as well for non-ideal flaws as for ideal flaws then it can be used without modification. If the sizing technique works differently for non-ideal flaws and this variation cannot be quantified, then the sizing technique cannot be used. In some cases, the technique performs differently for non-ideal flaws and this variation *is* quantified, e.g. the variation in scattered amplitude from cracks of the same size but different roughness values has been quantified [147]. In such cases, the sizing technique can still be used, provided the variation of the flaw from ideal e.g. its roughness, is quantified. This can be done using historical data on the types of flaws present in a particular component after certain operating conditions, or by using an NDT method on the actual flaw being investigated.

Being able to detect early stage damage in a component, prior to flaws actually forming, can be of great benefit because it helps with planning maintenance and guaranteeing safety [148]. Non-linear ultrasonics is a field of ultrasonics which measures the non-linearity in the elastic (stress-strain) response of materials which

is a property that increases when material is damaged; it has been found that non-linear techniques are more sensitive to identifying damage-related structural alterations than linear techniques are [149]. Non-linear ultrasonic imaging has been shown to be capable of detecting and quantifying very early stage failure (from approximately 15% of fatigue life) [148]. Non-linear ultrasonics can also be used to image closed cracks that are transparent to linear ultrasound [150]. Note that in Section 3 of this paper only linear ultrasonics was considered since non-linear ultrasonics is not widespread in industry; and this can be considered a remaining challenge.

Noisy materials cause problems because as well as scattering from flaws, there is significant scattering from material grain structure; various efforts have been made to simulate noise and also to reduce it [151–153]. As with non-ideal flaws, the performance of imaging and sizing techniques in non-ideal materials should be considered, as done in the comparison between TFM and the denoising algorithms [68]. Anisotropic materials are materials whose properties vary with direction; therefore the speed of sound in these materials varies with direction, making them another example of non-ideal materials. However, ultrasonic propagation and imaging in anisotropic materials has been studied in a lot of detail, in particular for welds [154], but also for composite materials [155] and single-crystal materials [156].

It is often the case in industrial settings that ultrasonic probes can only be placed on one surface of the component. Sometimes there are also limits to where the probe can be placed and to its maximum size. This leads to two issues: some parts of the flaw are not insonified; and some parts of the flaw are insonified but no scattered ultrasound reaches the probe. A lot of NDE researchers do take these limitations into account and try to overcome the resulting issues. For example, the back wall has been used as a mirror to image parts of a flaw that were previously not insonified [89,157] and to improve the inspection angles so that ultrasound from more of the flaw is captured [85]. However, further work is needed to understand how these techniques perform in very complicated component geometries, when component surfaces are rough and so on.

As already mentioned, surface-breaking cracks are of particular concern in industry [5]. It is sometimes the case that novel ultrasonic imaging techniques are only demonstrated on embedded flaws that are far from any component surface. Such flaws are a simpler case for two main reasons: there are no interactions with component surfaces, and embedded flaws can be horizontal and therefore oriented more favourably so that a lot of scattered energy is received back at the probe. It is good to see that in recent years, effort has been made on sizing surface-breaking flaws, in particular using Half-Skip imaging techniques [65,85,96]. Even some more advanced techniques focus on surface-breaking flaws e.g. [5,133,137]. In some cases, it is necessary to remove the signals from the back wall and there are various ways of doing this from simple subtraction [11] to more advanced techniques [133]. However, more needs to be done in terms of assessing the performance of the new sizing techniques (e.g. for tilted cracks) and making them robust enough to be used in industry.

A lot of work is published on sizing techniques but not always with statistically significant results and robust analysis of error. In fact, it is often the case that a new technique is proposed and demonstrated on just one or two flaw types and sizes. It would be beneficial to see more results where a new technique is trialled on different-sized flaws including ones where the technique does not perform well, so that the community can be aware of the technique's limits. A robust quantitative analysis, perhaps using one of the techniques described in Section 4, would be most beneficial. Obviously, if the technique is implemented in practice, any results published by researchers cannot be assumed to be valid for the particular application and further assessment will be required. However, the researchers' assessment and validation results can be an indicator of whether the technique is even worth implementing.

Looking outside NDE to software development and testing can be insightful. In software development, a V-model can be used to assess a new product; its name originates from its shape and also because two aspects which are included in it are Verification and Validation (p.181f in [158]). In verification, issues should focus on "Are we building the product right?", whilst in validation issues should focus on "Are we building the right product?" (p.165 in [158]). In NDE research it is often the case that some verification is performed e.g. we answer questions such as: "Do our experimental results match our simulated results?" and "Does our measured size equal the actual size?". However, we often do not fully address the next question and do not ensure the robustness, suitability and applicability of our sizing technique. In addition to performing a quantitative assessment, practicalities such as computing power and complexity of implementation must be considered, and industrial stakeholders should be consulted throughout the development of a new sizing technique.

6. Conclusion

This paper began with a description of the motivation behind sizing flaws and the suitability of ultrasonic testing for many applications. A review of established and more recent ultrasonic sizing techniques was then given. These were categorised into amplitude, temporal, imaging and inversion techniques. Different approaches for assessing sizing techniques were presented. Finally, remaining gaps and challenges in sizing flaws using ultrasound, were discussed. As well as pushing the boundaries in terms of resolution and being able to size smaller and smaller flaws, there is a need for more robust sizing techniques that can cope with non-ideal scenarios and therefore be applied with confidence in industry. It is particularly important for sizing techniques to become robust if flaw sentencing is to be done automatically.

As new ultrasonic techniques are developed, information about their suitability and performance for different flaw and material properties could be encapsulated in an expert system, as done for thermography [159]. As well as developing new ultrasonic techniques, combining different ultrasonic techniques [64,65], or fusing data from different NDE methods [160,161] might be ways forward.

Acknowledgements

References

[1] J.D. Achenbach, Quantitative nondestructive evaluation, Int. J. Solids Struct. 37 (2000) 13–27.
[2] M. Moles, Defect sizing in pipeline welds - what can we really achieve?, in: ASME/JSME Pressure Vessels and Piping Conference, 2004, San Diego.
[3] Health and Safety Executive, Information for the procurement and conduct of NDT – Part 4: Ultrasonic sizing errors and their implication for defect assessment, 2008.
[4] British Standards Institution, BS7910:2013+A1:2015 – Guide to methods for assessing the acceptability of flaws in metallic structures, 2016.
[5] A. Velichko, L. Bai, B.W. Drinkwater, Ultrasonic defect characterization using parametric-manifold mapping, Proc. Roy. Soc. A 473 (2017) 20170056.
[6] R. Halmshaw, Introduction to the Non-destructive Testing of Welded Joints, second ed., Abington Publishing, Cambridge, 1996.
[7] E.A. Ginzel, Automated ultrasonic testing for pipeline girth welds – a handbook, Advanced Practical NDT Series, 2006, Olympus NDT, Massachusetts.

[8] ASTM International, E164-13 – Standard practice for contact ultrasonic testing of weldments, 2013.
[9] ASTM International, E2700-14 – Standard practice for contact ultrasonic testing of welds using phased arrays, 2014.
[10] C. Nageswaran, C.R. Bird, Evaluation of the phased array transmit-receive longitudinal and time-of-flight diffraction techniques for inspection of a dissimilar weld, Insight - Non-Destr. Test. Cond. Monitor. 50 (12) (2008) 678–684.
[11] L. Satyanarayan et al., Investigations on imaging and sizing of defects using ultrasonic phased array and the synthetic aperture focusing technique, Insight - Non-Destr. Test. Cond. Monitor. 51 (7) (2009) 384–390.
[12] A. Chahbaz, R. Sicard, Comparative evaluation between ultrasonic phased array and synthetic aperture focusing techniques, AIP Conf. Proc. 657 (2003) 769–776.
[13] K. Kimoto, S. Ueno, S. Hirose, Image-based sizing of surface-breaking cracks by SH-wave array ultrasonic testing, Ultrasonics 45 (1–4) (2006) 152–164.
[14] O. Allan Kupcis, Detection, sizing and monitoring of defects by nondestructive evaluation: an overview, Can. Metall. Q. 19 (1) (1980) 23–34.
[15] P.A. Doyle, C.M. Scala, Crack depth measurement by ultrasonics: a review, Ultrasonics 16 (4) (1978) 164–170.
[16] B.W. Drinkwater, P.D. Wilcox, Ultrasonic arrays for non-destructive evaluation: a review, NDT&E Int. 39 (7) (2006) 525–541.
[17] J. Krautkrämer, H. Krautkrämer, Ultrasonic Testing of Materials, fourth ed., Springer-Verlag, Berlin, Heidelberg, 1990.
[18] D.E. Chimenti, Review of air-coupled ultrasonic materials characterization, Ultrasonics 54 (7) (2014) 1804–1816.
[19] C.B. Scruby, Some applications of laser ultrasound, Ultrasonics 27 (4) (1989) 195–209.
[20] T. Stratoudaki, M. Clark, P.D. Wilcox, Laser induced ultrasonic phased array using full matrix capture data acquisition and total focusing method, Opt. Express 24 (19) (2016) 21921–21938.
[21] J. Isla, F. Cegla, EMAT phased array: a feasibility study of surface crack detection, Ultrasonics 78 (2017) 1–9.
[22] ASTM International, E1316-17a – Standard terminology for nondestructive examinations, 2017.
[23] L. Bai, A. Velichko, B.W. Drinkwater, Characterization of defects using ultrasonic arrays: a dynamic classifier approach, IEEE Trans. Ultrason. Ferroelectr. Freq. Control 62 (12) (2015) 2146–2160.
[24] J.D. Hislop, Flaw size evaluation in immersed ultrasonic testing, Non-Destr. Test. 2 (3) (1969) 183–192.
[25] W. Kleinert, Defect Sizing using Non-destructive Ultrasonic Testing, Springer International Publishing, Cham, 2016.
[26] B.H. Lidington, D.H. Saunderson, M.G. Silk, Interference effects in the reflection of ultrasound from shallow slits, Non-Destr. Test. 8 (4) (1975) 185–190.
[27] W.C. Hitt, Progress in the field of non-destructive testing through the use of ultrasonics, in Symposium on Non-Destructive Testing, in: 55th Annual Meeting American Society for Testing Materials, 1953, American Society for Testing Materials: New York, pp. 53–75.
[28] A.N. Sinclair, et al, Manufacture of reference defects for NDE through Hot Isostatic Pressing, in: Review of Progress in Quantitative Nondestructive Evaluation, 1991, California.
[29] J. Krautkrämer, Determination of the size of defects by the ultrasonic impulse echo method, Br. J. Appl. Phys. 10 (6) (1959) 240–245.
[30] Olympus, Ultrasonic Flaw Detection Tutorial 8.2 DGS/AVG. Available from: <https://www.olympus-ims.com/en/ndt-tutorials/flaw-detection/dgs-avg/> (accessed 08.08.17).
[31] H. Wirdelius, E. Österberg, SKI Report 00:42 - Study of defect characteristics essential for NDT testing methods ET, UT and RT, 2000, Swedish Nuclear Power Inspectorate.
[32] M2M ndt, Total focusing method and phased-array technology. [Video], 2015. Available from: <https://www.youtube.com/watch?v=zOXgnBYcZqw> (accessed 08.08.17).
[33] M.V. Felice, Ultrasonic Array Inspections for Complex Defects, University of Bristol, Bristol, 2015.
[34] M.G. Silk, The use of diffraction-based time-of-flight measurements to locate and size defects, Br. J. NDT (May) (1984) 208–213.
[35] D.M. Corbly, P.F. Packman, H.S. Pearson, The accuracy and precision of ultrasonic shear wave flaw measurements as a function of stress on the flaw, Mater. Eval. (May) (1970) 103–110.
[36] B.G.W. Yee et al., Stress and the ultrasonic detection of fatigue cracks in engineering metals, Non-Destr. Test. 7 (5) (1974) 245–250.
[37] J.R. Birchak, C.G. Gardner, Comparative ultrasonic response of machined slots and fatigue cracks in 7075 Aluminium, Mater. Eval. (December) (1976) 275–280.
[38] P.P. Nanekar, B.K. Shah, Advanced ultrasonics for in-service inspection of nuclear plants, in: International Workshop on Imaging in NDE, 2007, IGCAR, Kalpakkam.
[39] M.G. Silk, B.H. Lidington, Defect sizing using an ultrasonic time delay approach, Br. J. NDT (March) (1975) 33–36.
[40] M.G. Silk, B.H. Lidington, The potential of scattered or diffracted ultrasound in the determinaton of crack depth, Non-Destr. Test. 8 (3) (1975) 146–151.
[41] M.G. Silk, The transfer of ultrasonic energy in the diffraction technique for crack sizing, Ultrasonics (May) (1979) 113–121.
[42] F.A. Ravenscroft, K. Newton, C.B. Scruby, Diffraction of ultrasound by cracks: comparison of experiment with theory, Ultrasonics 29 (1) (1991) 29–37.
[43] S. Baby et al., Time-of-flight diffraction (TOFD) technique for accurate sizing of surface-breaking cracks, Insight - Non-Destr. Test. Cond. Monitor. 45 (6) (2003) 426–430.
[44] A. Al-Ataby, W. Al-Nuaimy, O. Zahran, Towards automatic flaw sizing using ultrasonic time-of-flight diffraction, Insight - Non-Destr. Test. Cond. Monitor. 52 (7) (2010) 366–371.
[45] S. Baby et al., Time-of-flight diffraction (TOFD) technique for accurate sizing of cracks embedded in sub-cladding, Insight – Non-Destr. Test. Cond. Monitor. 45 (9) (2003) 600–604.
[46] B. Browne, Time of flight diffraction – its limitations – actual and perceived, NDTnet UTonline J. 2 (9) (1997).
[47] ASTM International, E2373/E2373M-14 – Standard practice for use of the ultrasonic time of flight diffraction (TOFD) technique, 2014.
[48] I. Komura et al., Crack detection and sizing technique by ultrasonic and electromagnetic methods, Nucl. Eng. Des. 206 (2–3) (2001) 351–362.
[49] O. Zahran, W. Al-Nuaimy, Automatic segmentation of time-of-flight diffraction images using time-frequency techniques – application to rail-track defect detection, Insight - Non-Destr. Test. Cond. Monitor. 46 (6) (2004) 338–343.
[50] W. Al-Nuaimy, O. Zahran, Time-of-flight diffraction – from semi-automatic inspection to semi-automatic interpretation, Insight – Non-Destr. Test. Cond. Monitor. 47 (10) (2005) 639–644.
[51] E.P. De Moura et al., Welding defect pattern recognition in TOFD signals Part 1. Linear classifiers, Insight – Non-Destr. Test. Cond. Monitor. 47 (12) (2005) 777–782.
[52] B.J. Engle, Quantitative Flaw Characterization with Ultrasonic Phased Arrays, Iowa State University, Iowa, 2013.
[53] E.A. Lloyd, An ultrasonic short-pulse shear-wave method for measuring the depth of surface-breaking cracks, Br. J. NDT (November) (1975) 172–175.
[54] F. Jacques, F. Moreau, E. Ginzel, Ultrasonic backscatter sizing using phased array – developments in tip diffraction flaw sizing, Insight – Non-Destr. Test. Cond. Monitor. 45 (11) (2003) 724–728.
[55] R.K. Chapman et al., Ultrasonic inspection of tilted defects using the 'corner effect' – modelling and experimental validation, Insight – Non-Destr. Test. Cond. Monitor. 50 (2) (2008) 66–69.
[56] P. Broberg, A. Runnemalm, M. Sjödahl, Improved corner detection by ultrasonic testing using phase analysis, Ultrasonics 53 (2) (2013) 630–634.
[57] M. Moles, L. Wesley, T. Sinclair, Accurate defect sizing using phased array and signal processing, in: 7th International Conference on NDE in Relation to Structural Integrity for Nuclear and Pressurized Components, 2009, Yokohama.
[58] B. Shakibi et al., Resolution enhancement of ultrasonic defect signals for crack sizing, NDT&E Int. 52 (2012) 37–50.
[59] T. Gang, Z.Y. Sheng, W.L. Tian, Time resolution improvement of ultrasonic TOFD testing by pulse compression technique, Insight – Non-Destr. Test. Cond. Monitor. 54 (4) (2012) 193–197.
[60] S.D. Kenny, K. Stamps, P. Crowther, Development of NDT techniques and inspection for detection and sizing of thermal fatigue cracking in steam-pipework bores of flexibly operated coal-fired power stations, Insight – Non-Destr. Test. Cond. Monitor. 45 (2) (2003) 125–129.
[61] R. Quimby, Practical limitations of TOFD on power station main steam pipework, Insight – Non-Destr. Test. Cond. Monitor. 48 (9) (2006) 559–563.
[62] A. Velichko, P.D. Wilcox, An analytical comparison of ultrasonic array imaging algorithms, J. Acoust. Soc. Am. 127 (4) (2010) 2377–2384.
[63] D. Pain, B.W. Drinkwater, Detection of fibre waviness using ultrasonic array scattering data, J. Nondestr. Eval. 32 (3) (2013) 215–227.
[64] J. Zhang et al., Investigation into distinguishing between small volumetric and crack-like defects using multi-view total focusing method images, AIP Conf. Proc. 2017 (1806) 040003-1–040003-7.
[65] J. Hörchens, C. Wassink, H. Haines, Ultrasound imaging of stress corrosion cracking, AIP Conf. Proc. 1650 (2015) 891–898.
[66] J. Zhang, B.W. Drinkwater, P.D. Wilcox, The use of ultrasonic arrays to characterize crack-like defects, J. Nondestr. Eval. 29 (4) (2010) 222–232.
[67] R.V. Murphy, Ultrasonic Defect-sizing using Decibel Drop Methods, Atomic Energy Control Board, Canada, 1987.
[68] J. Zhang, B.W. Drinkwater, P.D. Wilcox, Comparison of ultrasonic array imaging algorithms for nondestructive evaluation, IEEE Trans. Ultrason. Ferroelectr. Freq. Control 60 (8) (2013) 1732–1745.
[69] R.Y. Chiao, L.J. Thomas, Analytic evaluation of sampled aperture ultrasonic imaging techniques for NDE, IEEE Trans. Ultrason. Ferroelectr. Freq. Control 41 (4) (1994) 484–493.
[70] E. Hecht, A. Zajac, Optics, second ed., Addison-Wesley, Massachusetts, 1987.
[71] C. Fan et al., A comparison between ultrasonic array beamforming and super resolution imaging algorithms for non-destructive evaluation, Ultrasonics 54 (7) (2014) 1842–1850.
[72] J.R. Meyer-Arendt, Introduction to Classical and Modern Optics, second ed., Prentice-Hall, New Jersey, 1984.
[73] F. Simonetti, Localization of pointlike scatterers in solids with subwavelength resolution, Appl. Phys. Lett. 89 (9) (2006) 094105-1–094105-3.
[74] D. Nardoni et al., Sizing in the phased array technique using diffraction and amplitude displacement, Insight – Non-Destruct. Test. Cond. Monitor. 50 (10) (2008) 574–578.
[75] C. Holmes, B.W. Drinkwater, P.D. Wilcox, Post-processing of the full matrix of ultrasonic transmit–receive array data for non-destructive evaluation, NDT&E Int. 38 (8) (2005) 701–711.

[76] P.D. Wilcox, Ultrasonic arrays in NDE: beyond the B-scan, AIP Conf. Proc. 1511 (2013) 33–50.

[77] C. Holmes, B.W. Drinkwater, P.D. Wilcox, Advanced post-processing for scanned ultrasonic arrays: application to defect detection and classification in non-destructive evaluation, Ultrasonics 48 (6–7) (2008) 636–642.

[78] I.G. Pettigrew et al., Investigation of crack sizing using ultrasonic phased arrays with signal processing techniques, Insight – Non-Destr. Test. Cond. Monitor. 48 (2) (2006) 80–83.

[79] D.I.A. Lines, Rapid distributed data collection with arrays – the next step beyond full waveform capture, Insight – Non-Destr. Test. Cond. Monitor. 48 (2) (2006) 84–88.

[80] Diagnostic Sonar, FRD (including FMC+TFM) acquistion and display module, 2013. Available from: <http://www.diagnosticsonar.com/artman/publish/article_116.shtml> (accessed 23.08.17).

[81] G.A. Guarneri et al., A sparse reconstruction algorithm for ultrasonic images in nondestructive testing, Sensors (Basel) 15 (4) (2015) 9324–9343.

[82] S. Baby et al., Sizing of cracks embedded in sub-cladding using the ultrasonic synthetic aperture focusing technique (SAFT), Insight – Non-Destr. Test. Cond. Monitor. 46 (1) (2004) 26–30.

[83] P.D. Wilcox, C. Holmes, B.W. Drinkwater, Advanced reflector characterization with ultrasonic phased arrays in NDE applications, IEEE Trans. Ultrason. Ferroelectr. Freq. Control 54 (8) (2007) 1541–1550.

[84] S. Chatillon et al., Results of the 2014 UT modeling benchmark obtained with models implemented in CIVA: Solution of the FMC-TFM ultrasonic benchmark problem using CIVA, AIP Conf. Proc. 1650 (2015) 1847–1855.

[85] M.V. Felice, A. Velichko, P.D. Wilcox, Accurate depth measurement of small surface-breaking cracks using an ultrasonic array post-processing technique, NDT&E Int. 68 (2014) 105–112.

[86] A. Fidahoussen et al., Imaging of defects in several complex configurations by simulation-helped processing of ultrasonic array data, AIP Conf. Proc. 1211 (2010) 847–854.

[87] E. Iakovleva et al., Multi-mode TFM imaging with artifacts filtering using CIVA UT forwards models, AIP Conf. Proc. 1581 (2014) 72–79.

[88] J. Zhang et al., Defect detection using ultrasonic arrays: the multi-mode total focusing method, NDT&E Int. 43 (2) (2010) 123–133.

[89] T. Schmitte, et al., Application of the Total Focusing Method for improved defect characterization in the production of steel tubes, pipes and plates, in: 19th World Conference on Non-Destructive Testing, 2016, Munich.

[90] M.V. Felice et al., Depth measurement of small surface-breaking cracks using the half-skip total focusing method, AIP Conf. Proc. 1650 (2015) 994–1000.

[91] D. Duxbury, J. Russell, M. Lowe, Designing a calibrated full matrix capture based inspection, AIP Conf. Proc. 1335 (2011) 851–858.

[92] R. Long et al., Ultrasonic phased array inspection of flaws on weld fusion faces using Full Matrix Capture, AIP Conf. Proc. 1096 (2009) 848–855.

[93] S.F. Burch et al., M-skip: a quantitative technique for the measurement of wall loss in accessible components, Insight – Non-Destr. Test. Cond. Monitor. 49 (4) (2007) 190–194.

[94] X. Han, et al., Combination of direct, half-skip and full-skip TFM to characterize multi-faceted crack, in: IEEE International Ultrasonics Symposium, 2015, Taipei.

[95] G. Montaldo et al., Coherent plane-wave compounding for very high frame rate ultrasonography and transient elastography, IEEE Trans. Ultrason. Ferroelectr. Freq. Control 56 (3) (2009) 489–506.

[96] L. Le Jeune et al., Plane Wave Imaging for ultrasonic non-destructive testing: generalization to multimodal imaging, Ultrasonics 64 (2016) 128–138.

[97] A.J. Hunter, B.W. Drinkwater, P.D. Wilcox, The wavenumber algorithm for full-matrix imaging using an ultrasonic array, IEEE Trans. Ultrason. Ferroelectr. Freq. Control 55 (11) (2008) 2450–2462.

[98] A. Velichko, P.D. Wilcox, Reversible back-propagation imaging algorithm for postprocessing of ultrasonic array data, IEEE Trans. Ultrason. Ferroelectr. Freq. Control 56 (11) (2009) 2492–2503.

[99] N. Pörtzgen, Practical results of ultrasonic imaging by inverse wave field extrapolation, in: 9th European Conference on NDT, 2006, Berlin.

[100] N. Pörtzgen, D. Gisolf, G. Blacquière, Inverse wave field extrapolation: a different NDI approach to imaging defects, IEEE Trans. Ultrason. Ferroelectr. Freq. Control 54 (1) (2007) 118–127.

[101] J. Camacho, M. Parrilla, C. Fritsch, Phase coherence imaging, IEEE Trans. Ultrason. Ferroelectr. Freq. Control 56 (5) (2009) 958–974.

[102] G.E. Trahey, S.W. Smith, O.T. Von Ramm, Speckle pattern correlation with lateral aperture translation: experimental results and implications for spatial compounding, IEEE Trans. Ultrason. Ferroelectr. Freq. Control 33 (3) (1986) 257–264.

[103] F. Simonetti et al., Imaging beyond the Born approximation: an experimental investigation with an ultrasonic ring array, Phys. Rev. E 76 (3) (2007) 036601-1–036601-10.

[104] T. Hutt, Towards Next Generation Ultrasonic Imaging, Imperial College London, London, 2011.

[105] P.D. Wilcox, Optimization of array element pitch for NDE applications, AIP Conf. Proc. 1650 (2015) 952–961.

[106] E.A. Marengo, F.K. Gruber, F. Simonetti, Time-Reversal MUSIC imaging of extended targets, IEEE Trans. Image Process. 16 (8) (2007) 1967–1984.

[107] A. Kirsch, The MUSIC algorithm and the factorization method in inverse scattering theory for inhomogeneous media, Inverse Prob. 18 (4) (2002) 1025–1040.

[108] F. Simonetti, Multiple scattering: the key to unravel the subwavelength world from the far-field pattern of a scattered wave, Phys. Rev. E 73 (3) (2006) 036619-1–036619-13.

[109] D. Colton, A. Kirsch, A simple method for solving inverse scattering problems in the resonance region, Inverse Prob. 12 (4) (1996) 383–393.

[110] D. Colton, R. Kress, Using fundamental solutions in inverse scattering, Inverse Prob. 22 (3) (2006) R49–R66.

[111] A. Kirsch, Characterization of the shape of a scattering obstacle using the spectral data of the far field operator, Inverse Prob. 14 (6) (1998) 1489–1512.

[112] F. Cakoni, Recent developments in the qualitative approach to inverse electromagnetic scattering theory, J. Comput. Appl. Math. 204 (2) (2007) 242–255.

[113] C. Prada, F. Wu, M. Fink, The iterative time reversal mirror: a solution to self-focusing in the pulse echo mode, J. Acoust. Soc. Am. 90 (2) (1991) 1119–1129.

[114] M. Fink, Time reversal of ultrasonic fields – Part I: Basic principles, IEEE Trans. Ultrason. Ferroelectr. Freq. Control 39 (5) (1992) 555–566.

[115] F. Wu, J.L. Thomas, M. Fink, Time reversal of ultrasonic fields – Part II: Experimental results, IEEE Trans. Ultrason. Ferroelectr. Freq. Control 39 (5) (1992) 567–578.

[116] C. Prada, J.L. Thomas, M. Fink, The iterative time reversal process: analysis of the convergence, J. Acoust. Soc. Am. 97 (1) (1995) 62–71.

[117] M. Fink, C. Prada, Acoustic time-reversal mirrors, Inverse Prob. 17 (1) (2001) R1–R38.

[118] L.J. Cunningham et al., The detection of flaws in austenitic welds using the decomposition of the time-reversal operator, Proc. Roy. Soc. A 472 (2188) (2016) 20150500.

[119] S. Bannouf et al., Evaluation of multi-element methods applied to complex geometries, AIP Conf. Proc. 1430 (2012) 833–840.

[120] S. Robert, C. Prada, Ultrasonic flaw detection using the 1-bit DORT method, AIP Conf. Proc. 1096 (2009) 97–104.

[121] J. Zhang, B.W. Drinkwater, P.D. Wilcox, Defect characterization using an ultrasonic array to measure the scattering coefficient matrix, IEEE Trans. Ultrason. Ferroelectr. Freq. Control 55 (10) (2008) 2254–2265.

[122] G.S. Kino, The application of reciprocity theory to scattering of acoustic waves by flaws, J. Appl. Phys. 49 (6) (1978) 3190–3199.

[123] M.V. Felice et al., Obtaining geometries of real cracks and using an efficient finite element method to simulate their ultrasonic array response, Insight – Non-Destr. Test. Cond. Monitor. 56 (9) (2014) 492–498.

[124] L.W. Schmerr Jr., Fundamentals of ultrasonic nondestructive evaluation – a modeling approach, second ed., M.G. Cain, et al. (ed.), Springer Series in Measurement Science and Technology, 2016, Springer International Publishing, Switzerland.

[125] A. Velichko, P.D. Wilcox, A generalized approach for efficient finite element modeling of elastodynamic scattering in two and three dimensions, J. Acoust. Soc. Am. 128 (3) (2010) 1004–1014.

[126] A. Velichko, P.D. Wilcox, B.W. Drinkwater, Detection of near-surface and surface-breaking defects using ultrasonic arrays, AIP Conf. Proc. 1430 (2012) 929–936.

[127] J. Zhang, B.W. Drinkwater, P.D. Wilcox, Longitudinal wave scattering from rough crack-like defects, IEEE Trans. Ultrason. Ferroelectr. Freq. Control 58 (10) (2011) 2171–2180.

[128] L. Bai, A. Velichko, B.W. Drinkwater, Ultrasonic characterization of crack-like defects using scattering matrix similarity metrics, IEEE Trans. Ultrason. Ferroelectr. Freq. Control 62 (3) (2015) 545–559.

[129] Z. Wang et al., Image quality assessment: from error visibility to structural similarity, IEEE Trans. Image Process. 13 (4) (2004) 600–612.

[130] R. Malkin, M. Caleap, B.W. Drinkwater, A numerical database for ultrasonic defect characterisation using array data: robustness and accuracy, NDT&E Int. 83 (2016) 94–103.

[131] L.J. Cunningham et al., A spectral method for sizing cracks using ultrasonic arrays, Inverse Prob. Sci. Eng. 25 (12) (2017) 1788–1806.

[132] K.M.M. Tant, A.J. Mulholland, A. Gachagan, A model-based approach to crack sizing with ultrasonic arrays, IEEE Trans. Ultrason. Ferroelectr. Freq. Control 62 (5) (2015) 915–926.

[133] J. Zhang, P. Yu, T. Gang, Measurement of the ultrasonic scattering matrices of near-surface defects using ultrasonic arrays, Nondestr. Test. Eval. 31 (4) (2015) 303–318.

[134] N. Dominguez, V. Gibiat, Y. Esquerre, Time domain topological gradient and time reversal analogy: an inverse method for ultrasonic target detection, Wave Motion 42 (1) (2005) 31–52.

[135] R. Seidl, E. Rank, Iterative time reversal based flaw identification, Comput. Math. Appl. 72 (4) (2016) 879–892.

[136] R. Seidl, E. Rank, Full waveform inversion for ultrasonic flaw identification, AIP Conf. Proc. 2017 (1806) 090013-1–090013-7.

[137] E. Lubeigt et al., Topological imaging in bounded elastic media, Ultrasonics 76 (2017) 145–153.

[138] ASTM International, E2192-13 – Standard guide for planar flaw height sizing by ultrasonics, 2013.

[139] P.F. Packman et al., Definition of fatigue cracks through nondestructive testing, J. Mater. 4 (3) (1969) 666–700.

[140] R.K. Chapman, The assessment of defect measurement errors in the ultrasonic NDT of welds - Issue 1, 1987, Central Electricity Generating Board.

[141] M.A. Durivage, Practical Attribute and Variable Measurement System Analysis (MSA): A Guide for Conducting Gage R&R Studies and Test Method Validations, American Society for Quality, Wisconsin, 2015.

[142] X. Zhang, B. Chen, Y. Zhu, Application of measurement system R&R analysis in ultrasonic testing, in: 17th World Conference on Nondestructive Testing, 2008, Shanghai.

[143] D.-H. Lee et al., Analysis of round robin test for ultrasonic thickness measurement of wall thinned pipe in nuclear power plant, AIP Conf. Proc. 975 (2008) 1732–1738.

[144] J. Zhou et al., Improving the reliability of industrial multi-MW wind turbines, Insight – Non-Destr. Test. Cond. Monitor. 59 (4) (2017) 189–195.

[145] W. Cheng et al., Depth sizing of partial-contact stress corrosion cracks from ECT signals, NDT&E Int. 39 (5) (2006) 374–383.

[146] A.B. Woolridge et al., Ultrasonic detection and sizing of complex defects and implications for structural assessment procedures, Insight – Non-Destr. Test. Cond. Monitor. 45 (9) (2003) 594–599.

[147] J.R. Pettit, A.E. Walker, M.J. Lowe, Improved detection of rough defects for ultrasonic nondestructive evaluation inspections based on finite element modeling of elastic wave scattering, IEEE Trans. Ultrason. Ferroelectr. Freq. Control 62 (10) (2015) 1797–1808.

[148] J. Cheng et al., Monitoring fatigue crack growth using nonlinear ultrasonic phased array imaging, Smart Mater. Struct. 26 (5) (2017) 055006.

[149] K.E.-A. Van Den Abeele et al., Micro-damage diagnostics using nonlinear elastic wave spectroscopy (NEWS), NDT&E Int. 34 (4) (2001) 239–248.

[150] Y. Ohara et al., Ultrasonic measurement of closed stress corrosion crack depth using subharmonic phased array, Jpn. J. Appl. Phys. 48 (7S) (2009), p. 07GD01-1-07GD01-6.

[151] A. Van Pamel et al., Numerical simulations of ultrasonic array imaging of highly scattering materials, NDT&E Int. 81 (2016) 9–19.

[152] P.D. Wilcox, Array imaging of noisy materials, AIP Conf. Proc. 1335 (2011) 890–897.

[153] M. Li, G. Hayward, Ultrasound nondestructive evaluation (NDE) imaging with transducer arrays and adaptive processing, Sensors (Basel) 12 (1) (2012) 42–54.

[154] Z. Fan et al., Nonintrusive estimation of anisotropic stiffness maps of heterogeneous steel welds for the improvement of ultrasonic array inspection, IEEE Trans. Ultrason. Ferroelectr. Freq. Control 62 (8) (2015) 1530–1543.

[155] C. Li et al., Imaging composite material using ultrasonic arrays, NDT&E Int. 53 (2013) 8–17.

[156] C. Lane, The development of a 2D ultrasonic array inspection for single crystal turbine blades, Springer Theses – Recognizing outstanding Ph.D. research, 2014, Springer International Publishing, Switzerland.

[157] T.D. Hutt, F. Simonetti, Reconstructing the back of a defect from its mirror image, AIP Conf. Proc. 1211 (2010) 742–749.

[158] K. Mustafa, R.A. Khan, Software Testing - Concepts and Practices, Alpha Science International Ltd., Oxford, 2007.

[159] D.P. Almond, S.L. Angioni, S.G. Pickering, A case for NDT expert systems based on the development of the thermographic NDE advisory and guidance system, Insight – Non-Destr. Test. Cond. Monitor. 59 (9) (2017) 473–478.

[160] N. Brierley, T. Tippetts, P. Cawley, Data fusion for automated non-destructive inspection, Proc. Roy. Soc. A 470 (2167) (2014) 20140167.

[161] P. Daryabor, M.S. Safizadeh, Image fusion of ultrasonic and thermographic inspection of carbon/epoxy patches bonded to an aluminum plate, NDT&E Int. 90 (2017) 1–10.